Sustainable Food Technology

Accepted Manuscript

This article can be cited before page numbers have been issued, to do this please use: U. B and R. Paramasivam, *Sustainable Food Technol.*, 2025, DOI: 10.1039/D5FB00772K.

ROYAL SOCIETY OF CHEMISTRY

View Article Online
DOI: 10.1039/D5FB00772K

Gymnema sylvestre-Fortified Spheres and Beads from Waste Biomass: A Circular Bioeconomy Approach for Functional Food Delivery

In this work, two waste streams—chicken eggshells and brown seaweed (*Sargassum cinctum*)—are transformed into high-value functional food delivery platforms using circular bioeconomy concepts. Ionic gelation was used to extract and integrate calcium chloride (89.14% recovery) and sodium alginate (25% yield) to create *Gymnema sylvestre*-fortified spheres with pH-responsive release kinetics. The method demonstrated antidiabetic potential and generated 80.53% phenolic release at stomach pH by inhibiting α-amylase (30.1%) and α-glucosidase (31.1%). This trash-to-value approach offers biodegradable alternatives to petroleum-based packaging while addressing the 380 million tons of plastic waste generated yearly.

View Article Online
DOI: 10.1039/D5FB00772K

Gymnema sylvestre-Fortified Spheres and Beads from Waste Biomass: A Circular Bioeconomy Approach for Functional Food Delivery

Authors

Uthra Balasubramanian[a*], Dr Paramasivam Raajeswari [b]

Affiliation

[a]Ph.D. Scholar,
Department of Food Science and Nutrition,
Avinashilingam Institute for Home Science and Higher Education for Women,
Coimbatore – 641 043, Tamil Nadu, India
*E-mail: uthramanian29@gmail.com
Ph. No – 7904154886
ORCID ID- 0000-0003-1951-9745

[b]Professor,
Department of Food Science and Nutrition,
Avinashilingam Institute for Home Science and Higher Education for Women,
Coimbatore – 641 043, Tamil Nadu, India
E-mail: raajeswari_fsn@avinuty.ac.in
ORCID ID- 0000-0002-5311-0823

Gymnema sylvestre-Fortified Spheres and Beads from Waste Biomass: A Circular Bioeconomy Approach for Functional Food Delivery

Abstract

Novel circular bioeconomy approach for formulating functional food delivery platforms with antidiabetic potential by combining brown seaweed, *Sargassum cinctum*, avian eggshell waste, and *Gymnema sylvestre* extract. *S. cinctum* yielded a 25% of sodium alginate, whereas calcium chloride recovered from eggshells demonstrated 89.14% efficiency. FTIR spectroscopy confirmed structural integrity with characteristic carboxylate peaks (1600, 1400 cm^{-1}) for alginate and Ca-Cl stretching (689.66, 516.92 cm^{-1}) for calcium chloride. According to thermogravimetric analysis calcium chloride exhibited heat stability upto 700°C and alginate breakdown at 220–230°C. *G. sylvestre*-fortified spheres (3.87±0.31 cm) and beads (0.54±0.06 cm) were made by ionic gelation at an optimal sodium alginate concentration of 4%. The spheres had a total phenolic content of 27.77±1.29 mg GAE/g, a flavonoid content of 19.16±0.56 mg QE/g, and a nitric oxide scavenging activity of 72.66% at 10 mg/mL. At 100 µg/mL, enzyme inhibition tests showed α-amylase (30.1%) and α-glucosidase (31.1%) inhibition, which was much less than acarbose (>90%). Studies on pH-dependent release showed that phenol was released more quickly at pH 1.2 (80.53±0.87% by 120 min) and more slowly at pH 6.8 (59.13±0.83% by 180 min). Korsmeyer-Peppas investigation revealed anomalous transport mechanisms (n=0.94-0.98), and kinetic modelling revealed the Higuchi model as the best relevant descriptor (R^2>0.97). Despite lower taste scores (6.38-6.87), sensory analysis revealed acceptable consumer perception (total acceptability of 8.07-8.5 on a 9-point scale). This integrated approach effectively turns multiple waste streams into biodegradable functional carriers with pH-responsive release characteristics, even if bioactive loading adjustment is still required for commercial viability.

Keywords – Sodium alginate, Calcium chloride, Gymnema sylvestre, Spheres and beads, Circular economy, Waste valorisation

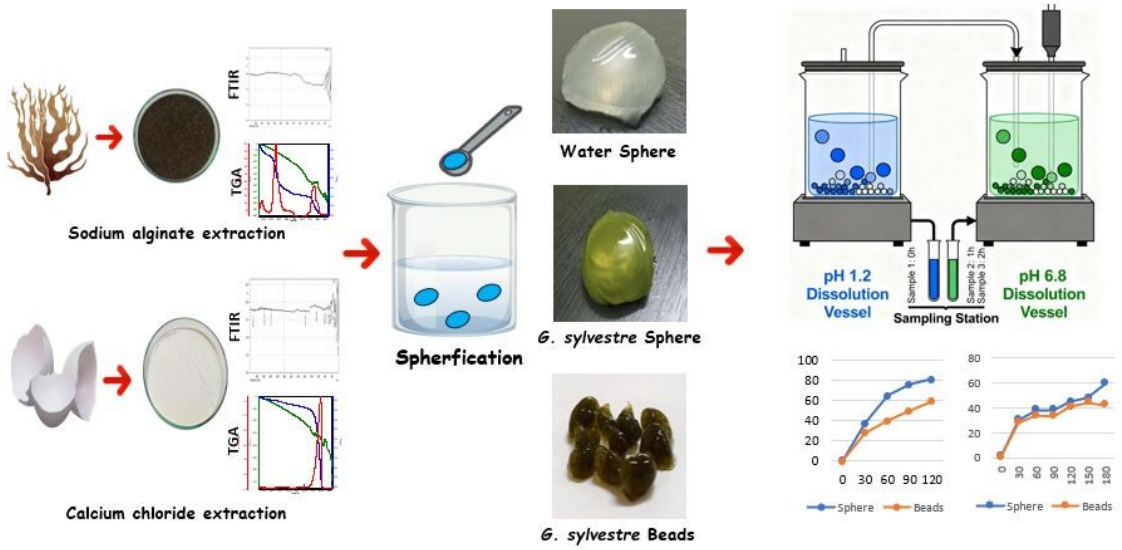

View Article Online
DOI: 10.1039/D5FB00772K

1 Introduction

The extensive use of plastic packaging has led to several environmental and economic problems, including resource depletion and ecosystem harm, with approximately 380 million tons of plastic packaging manufactured annually worldwide[1]. Economic studies indicate that cleaning up the world's plastic pollution by 2040 will cost between $18.3 and $158.4 trillion, including a notable 47% reduction in plastic production capacity[2]. Polyethene terephthalate (PET) accounts for 67% of the beverage packaging market because of its favourable physical properties, which include translucency, impact resistance, and barrier protection[3–6]. However, the environmental persistence of PET packaging has caused waste generation rates to rise from 12.84 to 1519.38 g/capita/year[7]. Beyond environmental concerns, PET packaging threatens people's health at risk by allowing toxins, including formaldehyde, acetaldehyde, bisphenol A, and antimony, into consumables[8–10]. To address these complicated difficulties, a paradigm shift from petroleum-based products to bio-based alternatives that are both commercially and environmentally viable is required. A practical strategy that reduces plastic pollution and adds value to underutilised waste streams is the production of biodegradable packaging materials from renewable biomass.

Biorefinery methods based on renewable biomass present intriguing opportunities for sustainable industrial systems. Biomass conversion technologies allow marine biomass, agricultural and animal waste to be converted into high-value goods through integrated processing systems that maximise resource utilisation while decreasing waste output[11]. Marine biomass, particularly derived from the seaweed industry, presents a significant possibility for the use of biorefineries. Approximately 600,000 tons of dried algal biomass are consumed annually by the seaweed industry, but only 15–30% of it is used effectively; the remaining 70–85% is discarded as waste[12]. Brown algae species like *Sargassum cinctum* are an underappreciated source of sodium alginate, a naturally occurring linear polysaccharide with significant potential for biomaterial applications[13–15]. Because of its unique functional properties, such as biodegradability, biocompatibility, and the ability to form gels through cross-linking with calcium ions, sodium alginate is highly beneficial for pharmaceutical and food packaging applications[16,17].

Similarly, avian waste, including eggshells, produces approximately one million tons of calcium-rich waste annually[18], an untapped resource for the production of sustainable calcium chloride[19,20]. Eggshell-derived calcium chloride offers an environmentally benign alternative to mined limestone[21] with predicted conversion yields of 94–97% and the potential to be scaled up to commercial production. Because of their unique properties, such as biocompatibility, a high surface-to-volume ratio, and the ability to exist in a range of morphologies and polymorphs, calcium chloride-based materials are great options for both industrial and biomedical applications[22].

A new possibility for the development of biorefineries, particularly for packaging applications, was presented by integrating two complementary biomass streams. The production of biodegradable spherical structures with adjustable characteristics is made possible by spherification, which is an innovative technique that involves crosslinking of alginate gels and calcium ions[23,24]. Functional additions such as *G. sylvestre* extract, a

View Article Online
DOI: 10.1039/D5FB00772K

medicinal herb with well-established therapeutic qualities, including suppression of sugar absorption, could be added to this process to improve it further [25]. Despite the fact that *G. sylvestre* has historically been taken as an aqueous herbal infusion, there are two inherent drawbacks to this format. When ingested in an untreated liquid form, gymnemic acids' complicated molecular architecture and lower lipid solubility limit intestinal absorption[26]. Furthermore, the delivery potential of a liquid infusion is limited because it cannot be integrated into commercial food matrices. Edible spheres and beads can be used for controlled intestinal release and bitterness masking to achieve acceptable palatability and to facilitate their incorporation into a variety of food products. Encapsulation with the extracted alginate, calcium chloride and *G. sylvestre* infusion of spheres and beads addresses the above-mentioned limitations and expands the functional reach of *G. sylvestre* beyond a traditional beverage[27].

Table 1 provides a comparative summary of recent studies cited using calcium alginate crosslinked delivery systems for functional ingredients, highlighting the alginate source, calcium source, encapsulated ingredient, and key findings to place the novelty of the current study in relation to existing literature.

Table 1 - Comparative overview of calcium alginate crosslinked delivery systems

Source of alginate	Source of calcium	Functional Ingredient Encapsulated	Delivery format	Remarkable Result	Reference
Extracted from brown seaweed *Sargassum polycystum* (Malaysia); alkaline extraction; yield 30.17%	Commercial $CaCl_2$ (ionic crosslinking of nanohybrid coating)	Quercetin (polyphenol) loaded into mesoporous silica nanoparticles (MSN) coated with extracted alginate	Alginate-coated nanoparticles (~415 nm)	EE 80.13%; pH-responsive release for colonic delivery; Sargassum alginate enhanced antioxidant stability of quercetin	28
Commercial sodium alginate (Sigma-Aldrich)	Commercial $CaCl_2$ (electrostatic extrusion gelation)	Thyme (*Thymus serpyllum*) aqueous polyphenol extract	Alginate gel beads (~730 µm) via electrostatic extrusion	EE 50–80%; FTIR confirmed no chemical reaction between alginate and polyphenols; intact bioactivity post-encapsulation	29
Commercial sodium alginate blended with commercial polyvinyl alcohol (PVA)	Commercial $CaCl_2$ + freeze-thaw crosslinking cycles	Curcumin (Curcuma longa bioactive compound)	CA/PVA hydrogel beads via ionic gelation	pH-sensitive release; minimal release at pH 1.2; enhanced intestinal release; EE ~90%; antibacterial and	30

View Article Online
DOI: 10.1039/D5FB00772K

				antioxidant activity confirmed	
Commercial sodium alginate (1–2% w/v) blended with whey protein	Commercial $CaCl_2$ (electrostatic extrusion)	Fennel (*Foeniculum vulgare*) essential oil	Calcium alginate microbeads (electrostatic extrusion + freeze-drying)	Optimal EE 51.95% with 1.5% alginate + 0.75% whey protein; whey protein improved EE; freeze-drying superior to air-drying; pH-sensitive swelling confirmed	31
Commercial sodium alginate (1.5% w/v) combined with carrageenan, agar, or gelatin hydrocolloids	Commercial $CaCl_2$ (5% w/v)	*Lactobacillus rhamnosus GG* (probiotic) + black goji berry (*Lycium ruthenicum*) polyphenols — co-encapsulation	Hydrocolloid-reinforced alginate beads	Alginate+gelatin beads showed the best LGG survival during GI digestion; co-digestion with milk enhanced TPC retention; hydrocolloid addition was critical for probiotic protection	32
Commercial sodium alginate (forming outer hydrogel bead)	Commercial $CaCl_2$ (mild ionic crosslinking)	Fucoxanthin (marine carotenoid from brown algae) pre-loaded into fucoidan/chitosan nanoparticles, then embedded in alginate beads	Two-step nanoparticle-in-hydrogel bead system	pH-responsive: <3.78% release at gastric pH 1.2; >99% at intestinal pH; double-protection enhanced fucoxanthin water solubility and GI stability	33

EE - Encapsulation Efficiency

Despite the research on calcium alginate-based encapsulation systems, three critical gaps persist. *G. sylvestre* has not been encapsulated in a food-grade alginate delivery system for functional food applications, nor has any study concurrently combined waste-derived calcium chloride and sodium alginate inside a single encapsulation platform. Furthermore, the impact of delivery geometry, bead versus spherical morphology, on pH-dependent release kinetics has not yet been thoroughly studied. By creating *G. sylvestre*-fortified spheres and beads from seaweed-extracted sodium alginate and eggshell-recovered calcium chloride within

View Article Online
DOI: 10.1039/D5FB00772K

a circular bioeconomy framework and assessing the impact of morphology on release behavior through mathematical kinetic modeling, the current study fills all three gaps.

This study aims to (i) optimize extraction parameters and yields for sodium alginate from *Sargassum cinctum* and calcium chloride from eggshells, (ii) characterize the physicochemical properties of extracted materials, and (iii) develop an integrated spherification process for creating edible spheres with functional enhancement through *G. sylvestre* extract incorporation. This approach offers eco-friendly alternatives to traditional plastic packaging while addressing waste management concerns in a range of industries. By creatively combining two distinct waste streams into a single biorefinery architecture, low-value biowaste is converted into high-value functional materials for food and pharmaceutical packaging applications. This strategy aligns with the principles of the circular bioeconomy by promoting resource efficiency and waste valorisation.

2 Materials and methods

2.1. Raw material

Sargassum cinctum was collected from Indian coastal regions that surround the Gulf of Mannar, a region known for its profusion of marine life. This seaweed species was chosen because of its high sodium alginate content, which is necessary for the production of biodegradable films. Hen eggshells, another crucial raw material, were sourced from household waste. *G. sylvestre*, widely known for its antidiabetic properties, was obtained from farmland in Tiruchirappalli, Tamil Nadu. Sodium carbonate and HCl were acquired from Sigma Aldrich.

Fig.1 Collection of *Sargassum cinctum* seaweed, harvested from the coastal waters of the Gulf of Mannar in India

2.2 Extraction of sodium alginate

The brown seaweed *Sargassum cinctum* was rinsed with tap water, allowed to dry in the shade, and then cut into pieces that were between 0.1 and 0.5 cm long[34]. The extraction procedure was altered as follows: 20 g of the sample was meticulously cleaned with distilled water and acidified for 24 hours using a 0.2 M HCl. The samples were then cleaned with

View Article Online
DOI: 10.1039/D5FB00772K

distilled water again before being extracted in 2% sodium carbonate solution at 30 to 40°C for five hours while stirring at 150 RPM. The supernatants collected after different extraction times were removed by centrifugation (Model: Kemi laboratory centrifuge, C8C). Sodium alginate was precipitated using ethanol. In the end, sodium alginate was purified twice using ethanol before being left to dry at room temperature.

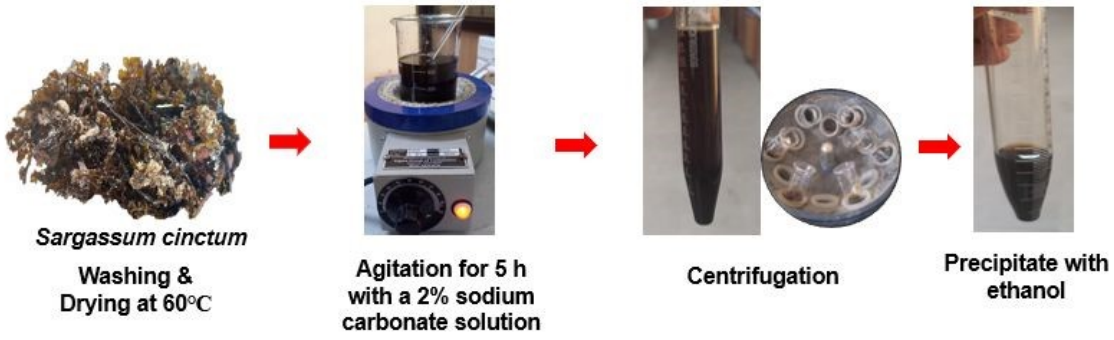

Fig.2 Sodium alginate extraction from *Sargassum cinctum*

2.3.Extraction of calcium chloride

Eggshells underwent a multi-step disinfection procedure before calcium chloride extraction to guarantee the product's microbiological safety for use in food-grade applications. After washing the shells under running water to remove any of the organic debris on the surface, they were submerged in 70% (v/v) ethanol for 15 minutes at room temperature and then cleaned three times with sterile distilled water. In accordance with procedures described for pharmacopeial-grade eggshell calcium carbonate isolation, eggshells were then oven-dried for two hours at 200°C to accomplish thermal inactivation of any remaining bacteria [35]. Ten g of crushed eggshells with 50 mL of 2M HCl solution. The mixture was then periodically stirred until no gas bubbles were visible, which took three hours. The mixture was centrifuged at 1774 × g for 10 minutes to produce calcium chloride crystals or eggshell calcium chloride. The supernatant was then separated and heated to 110–115°C until it dried [36].

2.4.Preparation of *G. sylvestre* infusion

G. sylvestre infusion was extracted by heating 1 g of powdered plant sample in 10 mL of distilled water for 30 min at 80°C. The infusion was filtered using Whatman filter paper (Grade 40, ashless) and centrifuged at 6000 rpm for 5 min, and the supernatant was used for spherification [37].

2.5.Physicochemical analysis for extracted sodium alginate and calcium chloride

The moisture and ash content of the extracted sodium alginate and calcium chloride samples were measured in triplicate, with results as mean±SD [38]. The functional groups in the extracted sodium alginate and calcium chloride were identified using FTIR spectroscopy. Shimadzu FTIR equipment was used for the analysis, and scans were made at a resolution of 4 cm^{-1} between 400 and 4000 cm^{-1}. The mannuronic to guluronic acid (M/G) ratio of the extracted sodium alginate was estimated from the FTIR spectrum using the baseline absorbance

View Article Online
DOI: 10.1039/D5FB00772K

method[39]. The absorbance values at the characteristic wavenumbers of 1033 cm^{-1} (mannuronic acid, M) and 1080 cm^{-1} (guluronic acid, G) were calculated using the following expression:

$$A = \log(\text{T\_baseline} / \text{T\_peak})$$

T_baseline represents the transmittance at the reference baseline at 1200 cm^{-1}, and T_peak represents the transmittance at the respective characteristic wavenumber. The M/G ratio was subsequently determined as:

$$M/G\ ratio\ =\ A(M)\ /\ A(G)$$

A Thermogravimetric Analyser (TG/DTA, EXSTAR/6300) was used to assess the thermal characteristics of the extracted sodium alginate and calcium chloride. TGA determines the weight loss of a material as it is heated, revealing the details of its moisture loss, breakdown temperature, and thermal stability[40]. The physicochemical properties of the extracted sodium alginate and calcium chloride were evaluated against internationally accepted standards: the United States Pharmacopeia-National Formulary (USP-NF), the European Pharmacopoeia (EP 7.0, Sodium Alginate Monograph No. 0625), and the Food Chemicals Codex (FCC 13, Sodium Alginate INS 401; Calcium Chloride Monograph), which represent the primary purity and safety benchmarks for food-grade and pharmaceutical excipient applications [41–44].

2.6.Standardisation of *G. sylvestre* edible spheres and beads

Two distinct methodologies and different concentrations were employed for formulating edible spheres and beads. Sodium alginate was taken in various concentrations, and the solution (1,2,3,4, and 5 %w/v) was made by carefully stirring for 15 mins and then letting it sit for 30 mins to release trapped air. For the cross-linking bath, 1% calcium chloride solution (5 g in 500 mL of water) was created concurrently. 20 mL of *G. sylvestre* infusion was evenly distributed throughout the alginate matrix for the preparation of the *G. sylvestre* edible sphere and beads. Preparation of water and *G. sylvestre* spheres, the alginate solution was dropped with the help of a curved spoon into a calcium chloride solution and continuously stirred until the formation of spheres. For the uniform *G. sylvestre* bead production, the syringe was used to drop into the alginate solution. Upon contact with the Ca^{2}-rich environment, instantaneous interfacial gelation occurred through the formation of "egg-box" structures, with the nascent matrices maintained in the gelation medium for 5 minutes to ensure complete cross-linking throughout the polymeric network [45,46]. The spheres and beads' diameters were measured using a vernier calliper.

View Article Online
DOI: 10.1039/D5FB00772K

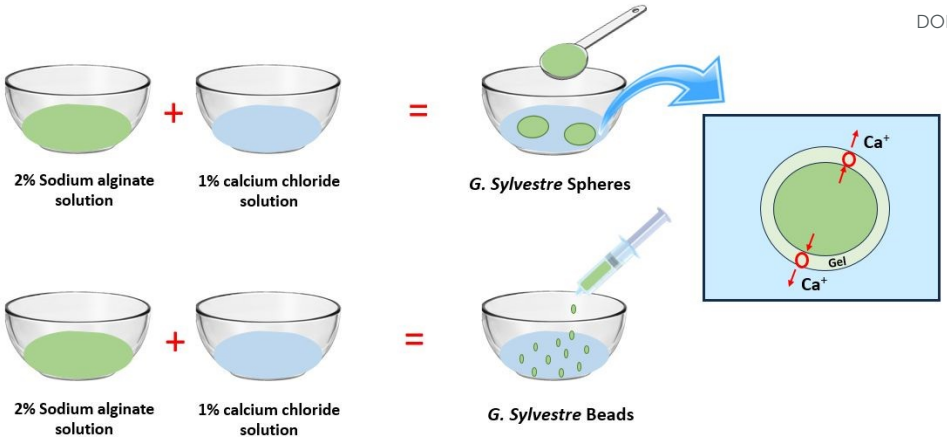

Fig.3 Preparation of *G. sylvestre* spheres and beads using spherification

2.7.Soxhlet Extraction

The edible sphere and bead sample was extracted from methanol using a Soxhlet apparatus (250 ml capacity, Sl. No.122). 5 g of the sample material was extracted with methanol using a Soxhlet thimble (Model: 64840-U) for 12 hours, and the concentrated residue was obtained by evaporating the methanol under reduced pressure. The residue was then reconstituted in methanol to the required concentration to obtain the crude extract for further analysis [47].

2.8.Total Phenol Compounds (TPC)

The Folin-Ciocalteu method was used to determine the total phenol content of the *G. sylvestre* sphere and beads. Briefly, 100 µl of extract was mixed with 400 µl of water and 150 µl of Folin-Ciocalteu reagent. The content was mixed thoroughly, and after 3 min, 500 µl of sodium carbonate solution was added. After 2 h at room temperature in the dark, the absorbance was measured at 750nm using a UV-Vis spectrophotometer (Shimadzu UV-1900). The results were expressed as mg GAE (gallic acid equivalents)/g extract [48].

2.9.Total Flavonoid Content (TFC)

The total flavonoid content was assessed using the aluminium chloride method as described in a previous reference. Briefly, 100 µl of extract was mixed with 400 µl of methanol and 100 µl of 10% $AlCl_3$, and 100 µl of NaOH (1M) was added. The solution was mixed and measured at 450 nm. The findings were expressed as mg quercetin equivalents (QE)/g of extract [49].

2.10. Antioxidant Activity

The nitric oxide radical scavenging activity of the sphere and beads was determined according to the method described by sodium nitroprusside (5 mM) in standard phosphate buffer saline solution (0.025 M, pH 7.4), which was incubated with different concentrations of the sample and ascorbic acid, and the tubes were incubated at 25 °C for 5 hr. After 5 h, 0.5 ml of the incubation mixture was removed and diluted with 0.5 ml of Griess reagent. The absorbance of the chromophore formed during diazotization of nitrite with sulphanilamide and its subsequent coupling with naphthyl ethylene diamine was read at 546 nm, and the percentage

View Article Online
DOI: 10.1039/D5FB00772K

inhibition was calculated as follows,

$$\%\ scavenging\ activity = Ac - As/Ac \times 100$$

Where Ac is the absorbance of the control, and As is the absorbance of the sample[50].

2.11. α-Amylase inhibition assay

This study evaluated the α-amylase and α-glucosidase inhibitory capabilities of the sphere and bead formulations at doses ranging from 10 to 100 µg/mL using acarbose as a reference standard. The mixture was preincubated for 10 mins at 25°C after different concentrations of the sample extract were added to 100 µl of 0.02 M sodium phosphate buffer (pH 6.9) and 100 µl of α-amylase solution (4.5 Units/mL/min). 1.0 mL of dinitrosalicylic acid reagent was added to stop the reaction after 30 mins of incubation at 25°C with 100 µl of 1% starch solution. The test tubes were incubated in a boiling water bath (Model: WB159910-33) for five minutes before being allowed to cool to room temperature. By comparing the results to the control, which has a buffer instead of an extract, the percentage of α-amylase enzyme inhibition was ascertained [51].

2.12. α-glucosidase inhibition assay

Different quantities of the sample extract were prepared and preincubated for five minutes at 25°C using 100 µl of 0.1 M phosphate buffer (pH 6.9) and 100 µl of α-glucosidase solution (1 Unit/mL/min). The mixture was incubated at 25°C for 10 minutes after 100 µl of p-nitrophenyl-α-D-glucopyranoside (5 mM) was added. Absorbance measurements were made at 405 nm after the incubation period, and the results were calculated and displayed as a percentage[51].

2.13. pH-dependent drug release

The dissolution medium at pH 1.2 was prepared by dissolving 2.0 g of sodium chloride in 7.0 mL of concentrated hydrochloric acid, followed by dilution to a final volume of 1000 mL with distilled water. The pH of the prepared solution was verified using a calibrated pH meter to ensure it remained within the specified range of 1.2 ± 0.1. Sodium phosphate buffer was prepared, and the pH was adjusted to 6.8 ± 0.1 using either dilute hydrochloric acid or sodium hydroxide solution as required. The pH of the buffer solution was verified using the calibrated pH meter before use in the dissolution experiments. One gram of the sphere formulation was added to 100 mL of pH 1.2 HCl solution and pH 6.8 phosphate buffer solution in a dissolution vessel maintained at 37°C ± 0.5°C. One gram of the bead formulation was concurrently added to a separate 100 mL aliquot of the same pH 1.2 medium and pH 6.8 solution at the same temperature. Samples were carefully collected from both vessels at predetermined intervals of 30, 60, 90, and 120 minutes. At each time point, a 1 mL aliquot was taken out and replaced with a 1 mL pH solution using a sterile syringe. Through further examination, the phenol and flavonoid content of the filtered samples was determined. Phenol content was quantified by UV-Vis spectrophotometry using the Folin-Ciocalteu method with gallic acid as the standard reference material, following appropriate dilution to ensure concentrations remained within the linear range of the calibration curve. Flavonoid content was determined using the aluminium chloride colourimetric method with quantification by UV-Vis

View Article Online
DOI: 10.1039/D5FB00772K

spectrophotometry at the appropriate wavelength of maximum absorption (λmax). All concentrations were determined by reference to their respective established calibration curves[52]. The dissolution data were theoretically modelled using four popular kinetic models[53,54].

Zero-Order Kinetics - $Qt = Q_0 + K_0 t$

First-Order Kinetics - $\log Qt = \log Q_0 + K_1 t/2.303$

Higuchi Model - $Qt = KH\sqrt{t}$

Korsmeyer-Peppas Model - $\frac{Mt}{M\infty} = Ktn$

2.14. Sensory evaluation

A consumer panel comprising 30 female participants (n=30), aged 20–30 years, participated in the sensory evaluation. To determine baseline consumer approval, panellists used a standardised 9-point hedonic scale to evaluate the organoleptic qualities of spheres and beads (1 = severely disliked and 9 = greatly liked). To avoid positional bias, three-digit random codes were used to represent each sample in a randomised counterbalanced order. The participants evaluated the samples based on various parameters.

2.15. Statistical analysis

Statistical analysis of the sensory data was conducted with IBM SPSS software, version 25, and means of the panel member hedonic attribute data were analysed at a 95% confidence level using one-way analysis of variance (ANOVA) and Duncan's Multiple Range Test (DMRT).

3 Results and discussion

3.1. Yield of sodium alginate

The extraction process started with 20 g of raw material and produced 5 g of purified sodium alginate (Fig.4a) with a yield efficiency of 25% (w/w). This yield falls within the reported range for brown algae species (20–65%), which varies considerably depending on extraction parameters (temperature, pH, sodium carbonate concentration, and extraction duration) and algal species. Comparative studies have demonstrated higher yields: *Sargassum polycystum* achieved 37.56% extraction efficiency using 7.0% sodium carbonate, while *Lobophora variegata* and *Cystoseira implexa* yielded 29.15% and 27.57%, respectively [55,56]. The moderate yield obtained in the present study may be attributed to the lower sodium carbonate concentration employed to minimise chemical usage.

3.2. Yield of calcium chloride

An 89.14% (w/w) conversion efficiency was achieved by the production of 8 g of calcium chloride (Fig.4b) from 10 g of crushed eggshells, and this result aligns with previous studies. This high recovery rate demonstrates the effectiveness of the acid-mediated conversion of calcium carbonate to calcium chloride and indicates that the inorganic calcium component of the eggshell matrix is almost entirely dissolved. Based on the research, an improved acid-

View Article Online
DOI: 10.1039/D5FB00772K

dissolving procedure to extract calcium chloride in an outstanding yield of 87.38% (w/w) 57. According to Domrongpokkaphan *et al*. (2022), a conversion efficiency of 86.52% (w/w) was achieved by extracting 16.07 g of anhydrous $CaCl_2$ from 20 g of eggshell waste [58].

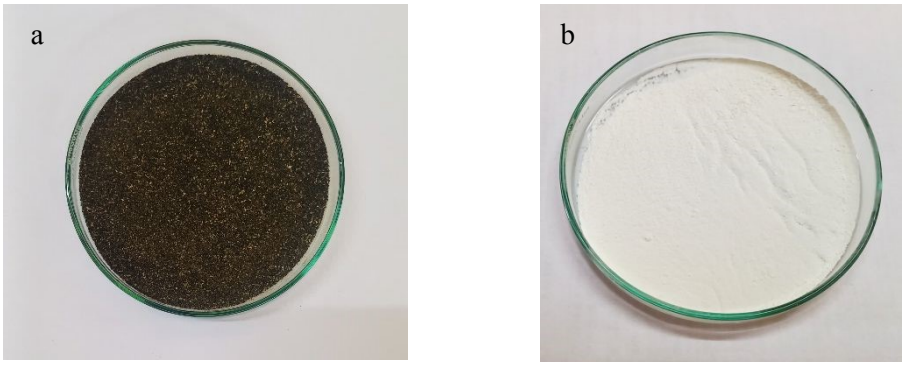

Fig.4(a) Extracted sodium alginate from *Sargassum cinctum* 3(b) extracted calcium chloride from eggshell

3.2 Moisture content (MC)

Analysis of the moisture content of sodium alginate and calcium chloride revealed significantly lower values than comparable literature values; sodium alginate moisture content was 3.15 ± 0.43% (Table -2), and that of calcium chloride was 2.82 ± 0.17%. The moisture content obtained was lower than the Codex specification of 15% and comparable to industrial-grade sodium alginate [59]. While earlier research on calcium chloride extracted from eggshells reported a moisture content of 0.98%, the moisture measurement followed the conventional AOAC methodology, which involves precise gravimetric analysis through mass loss following heating at 105 ± 1°C for 24 h [57,60]. Moisture content of extracted sodium alginate (3.15 +/- 0.43%) and calcium chloride (2.82 +/- 0.17%) complied with the respective USP-NF, EP, and FCC specifications of NMT 15.0% and NMT 5.0%.

3.3 Ash content (AC)

Relevant data on the mineral composition and extraction efficiency of materials obtained from biomass were revealed by the ash content analysis of extracted sodium alginate and calcium chloride. Ash content values of 15.21 ± 0.32% for sodium alginate and 89.18 ± 0.61% for calcium chloride were found in the current investigation; these values are significantly different from those found in the comparative literature. The observed ash level for sodium alginate showed a significant variation in the mineral content generated from seaweed biomass, falling within the wider range of 14.25%-26.57%[61]. A study of eggshell powder revealed a comparatively high ash level of 93.26%, demonstrating the distinct mineralogical properties of various biomass sources[62]. The ash content of sodium alginate (15.21 +/- 0.32%) exceeded the pharmacopeial limit of NMT 4.0% (sulphated ash), attributable to inherent mineral co-extraction from marine biomass, a well-documented characteristic of crude seaweed-derived alginate (reported range: 14.25-26.57%) and identifies purification as a prerequisite for pharmaceutical-grade application.

View Article Online
DOI: 10.1039/D5FB00772K

Table -2 Physicochemical values for sodium alginate and calcium chloride

Sample	Yield %	Moisture %	Ash %
Sodium alginate	25	3.15 ± 0.43	15.21 ± 0.32
Calcium chloride	89.14	2.82 ± 0.17	89.18 ± 0.61

Results are expressed in Mean ± S.D (n=3).

3.4 Fourier Transform Infrared Spectroscopy (FTIR)

Table – 3 and Fig. 5 (a.b) demonstrate the peaks of the functional group of sodium alginate and calcium chloride. FTIR-confirmed characteristic carboxylate peaks (1600, 1400 cm-1) and absence of free carboxylic acid at 1710-1730 cm-1 satisfy the identification criteria of all three pharmacopoeias for sodium alginate, while Ca-Cl stretching vibrations (689.66 and 516.92 cm-1) confirm chemical identity of calcium chloride per USP and EP requirements. Sodium alginate is a linear polysaccharide composed of two uronic acid monomers: β-D-mannuronic acid (M units) and α-L-guluronic acid (G units), arranged in three distinct block sequences [63]. The unit of sodium alginate has the formula $(C_6H_7NaO_6)$ with an average monomer molecular weight of 216.12 g/mol. The two constituent sugar monomers share the same molecular formula ($C_6H_{10}O_7$) and an identical molecular weight of 194.14 g/mol each (CAS: 6906-37-2 for β-D-mannuronic acid; CAS: 15769-56-9 for α-L-guluronic acid)[64]. According to literature reports, the molecular weight (Mw) of sodium alginate isolated from the genus Sargassum has been reported to range from 4.73×10^4 g/mol to 5.53×10^5 g/mol, depending on the collection and extraction methods used. The molecular weight of alginate isolated from *Sargassum polycystum* was shown to be 4.73×10^4 g/mol using the Mark-Houwink-Sakurada viscometry technique[65]. Sodium alginate isolated from *S. natans* in the Caribbean was measured at a molecular weight of 3.14×10^5 g/mol using GPC-NMR[66]. Similarly, the molecular weight of sodium alginate from *S. muticum* was quantified at 2.02×10^5 g/mol (202 kDa) using SEC-MALLS[67]. The FTIR-based estimation of the M/G ratio of the extracted *S. cinctum* sodium alginate yielded a value of 1.49, indicating a dominance of mannuronic acid residues over guluronic acid in the polymer chain. This value is consistent with M/G ratios previously reported for alginates derived from *Sargassum* species, which typically range between 1.04 and 4.41. A higher M/G ratio is known to favour the formation of soft, flexible, and elastic hydrogel matrices, which is particularly advantageous for the encapsulation and controlled release of bioactive compounds in pharmaceutical and functional food applications[68].

Table -3 FTIR Spectra for sodium alginate and calcium chloride

Sample	Wavenumber (cm^{-1})	Functional Group	Vibration Mode	Interpretation
Sodium alginate [69,70]	3200-3600 (broad)	O-H	Stretching	Extensive hydrogen bonding networks (intra- and intermolecular) characteristic of polysaccharides indicate absorbed moisture and hydroxyl groups

	2800-3000 (weak)	C-H	Stretching	Aliphatic C-H from pyranose ring structures of mannuronic and guluronic acid residues; low intensity typical for polysaccharides
	1600	COO^-	Asymmetric stretching	carboxylate ion presence, indicating complete neutralisation to the sodium salt form
	1400	COO^-	Symmetric stretching	Paired with 1600 cm^{-1} peak; ~200 cm^{-1} separation confirms ionic sodium salt character
	1000-1100 (strong, broad)	C-O-C,C-O	Glycosidic linkage stretching; pyranose ring C-O stretching	Characteristic polysaccharide backbone signal; reflects β-1,4-glycosidic bonds connecting uronic acid monomers
	800-900 (fingerprint)	C-O	Various (M-block: ~884 cm^{-1}; G-block: ~939 cm^{-1})	Mannuronic/guluronic acid-specific bands would indicate M/G block ratio
	Absence at 1710-1730	C=O	Carbonyl stretching	Absence confirms no residual alginic acid (carboxylic acid form); validates complete alkaline conversion
Calcium chloride[22]	3842.20,	O-H	Stretching	Sharp, distinct hydroxyl stretching vibrations indicate crystalline water or surface-adsorbed moisture; it differs from the broad alginate O-H band due to a more ordered structure
	2970.38	C-H	Stretching	Weak aliphatic C-H stretching
	948.98	Ca-O	Calcium-oxygen stretching	Critical peak confirming calcium-oxygen bonding; validates the presence of calcium
	686.66	Ca-Cl	Stretching	Diagnostic peak for calcium chloride; confirms successful chloride formation through acid-mediated conversion
	524.64	Ca-Cl	Stretching (fingerprint)	Strong Ca-Cl vibration in fingerprint region; validates chemical identity as calcium chloride; intensity suggests substantial $CaCl_2$ formation

View Article Online
DOI: 10.1039/D5FB00772K

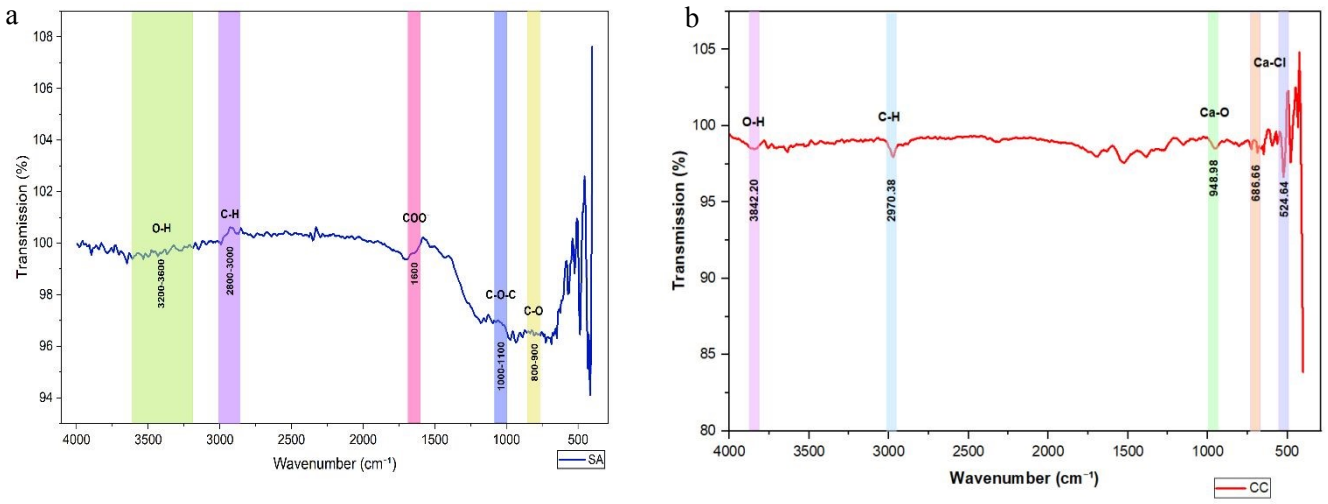

Fig.5 FTIR spectra of extracted **(a)** sodium alginate and **(b)** calcium chloride

3.5 Thermogravimetric Analysis (TGA)

Its intrinsic hydrophilicity was highlighted by the sodium alginate thermal profile, which showed a multistage breakdown process with an initial weight loss of 50–120°C to surface and bound water evaporation. The depolymerisation of alginate chains through glycosidic bond cleavage and decarboxylation of uronic acid residues was reflected in the most significant thermal event, which took place between 220 and 230°C and was marked by a pronounced DTG peak and a steep TG curve decrease (Fig. 6a). The literature demonstrates a weight loss trend that is comparable to commercial sodium alginate samples, with a noticeable weight decrease between 250 and 300°C and a slower rate of disintegration between 300 and 750°C[71].

The calcium chloride that was extracted from the eggshell, on the other hand, showed a noticeable breakdown phase at 750-775°C, which was marked by a rapid mass loss of 35-40% and a progressive weight loss of 10-15% up to 700°C (Fig.6b). Earlier studies showed mass losses of 21% up to 260°C, a comparatively steady mass of 79% until 800°C, and further declines during the heating and cooling phases. Complex structural reorganization and phase transitions are suggested by the endothermic transitions observed in both materials, especially the numerous tiny changes in the calcium chloride DTA curve between 600 and 700°C. The existence of inorganic components and the possible creation of stable calcium-based compounds were indicated by the residual mass of 45–50% for calcium chloride and an entire mass loss of 75–80% for sodium alginate at 900°C[72].

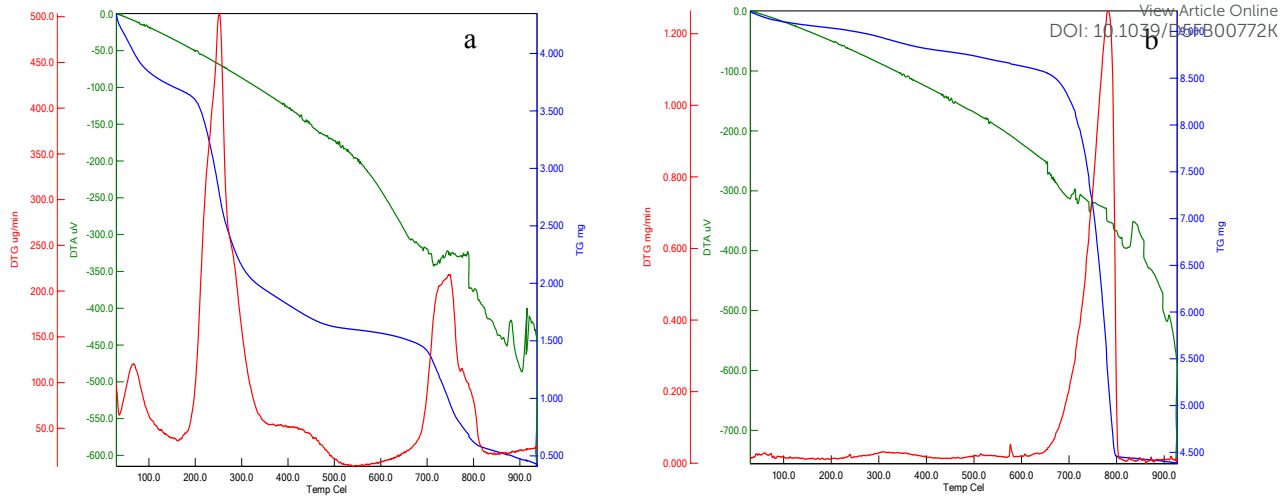

Fig.6 TGA curve of extracted **(a)** sodium alginate and **(b)** calcium chloride

3.6 Optimisation of spheres and beads

The findings show a distinct relationship between the reactant concentrations and the structural integrity of the resulting products (Table-4). The structural stability and spherical diameter of the water spheres were directly correlated with sodium alginate content. In particular, only a thin layer with inadequate structural integrity developed at a concentration of 1 %. When the concentration was increased to 2%, well-formed spheres with a thin layer of liquid-containing calcium alginate with a measured 3.64±0.10 cm in diameter appeared [46]**.** Subsequently, further increases to 3%, 4%, and 5% produced progressively larger spheres with improved structural properties that ranged from well-formed to thick-layered and finally hardened structures at the highest concentration [73].

G. sylvestre spheres showed comparable patterns of concentration-dependent formation patterns. At 1% sodium alginate, no spheres were formed; however, at 2% sodium alginate, a thin layer was formed. Well-formed spheres measuring 3.26±0.70 cm showed optimal formation at 3 and 4%. With diameters of 3.87±0.09, thicker layers and firm gel formation were the outcomes of higher concentration. The *G. sylvestre* bead trials demonstrated that successful bead formation required a minimum sodium alginate concentration of 2%, below which only thin layers formed without a proper bead structure. At 2 and 3%, beads were well-formed, but increasing concentrations to 4 and 5% produced progressively larger and more structurally robust beads, with diameters ranging from 0.63±0.02 and 0.67±0.05 cm, ultimately achieving hard bead formation at the highest concentrations.

To balance the structural integrity with the desired physical qualities, these results imply that the ideal sodium alginate concentration for sphere and bead production is between 3% and 4%. While excessive hardening at higher concentrations (5%) may be undesirable for some applications requiring specific textural features, unsuccessful production at lower concentrations (1%) indicates inadequate cross-linking with calcium chloride. In contrast, earlier research revealed spheres that ranged in size from 49.3 to 52.1 mm and had a sphericity index of 0.98 to 1.00. Furthermore, 1% w/v calcium lactate gluconate, 1% w/v sodium alginate, and a 10-minute sphere-forming period that produced a sphere thickness of 0.46 mm and

mechanical strength of 0.94 N/mm² were the justified preparations for encapsulating energy beverages by reverse spherification [74].

Table – 4 Effect of Sodium alginate and calcium chloride concentration on sphere formation and diameter

Variation	Sodium alginate (%)	Calcium chloride (%)	*G. sylvestre* infusion (mL)	Gelling time	Sphere formation	Sphere Diameter(cm)
WS	1	1	0	5	Thin layer formed	-
WS	2	1	0	5	Well formed	2.64±0.10[a]
WS	3	1	0	5	Well formed	2.76±0.17[a]
WS	4	1	0	5	Well formed	3.26±0.70[b]
WS	5	1	0	5	Hard layer formed	3.87±0.09[c]
GS	1	1	20	5	Incomplete gel formation	-
GS	2	1	20	5	Thin layer formed	-
GS	3	1	20	5	Well formed	1.87±0.31[a]
GS	4	1	20	5	Well formed	2.2±0.19[a]
GS	5	1	20	5	Hard gel	2.86±0.10[b]
GB	1	1	20	5	Incomplete gel formation	-
GB	2	1	20	5	Beads well formed	0.41±0.04[a]
GB	3	1	20	5	Well formed	0.54±0.06[b]
GB	4	1	20	5	Hard beads	0.63±0.02[b]
GB	5	1	20	5	Hard beads	0.67±0.05[c]

Mean ± S.D (n=3). The letters a, b, and c in superscript refer to the significant difference values ($P < 0.05$). WS- Water Sphere, GS – *G. sylvestre* Sphere, GB – *G. sylvestre* Beads

3.7 *G. sylvestre* spheres and beads

Based on optimal formation parameters, the resultant spheres and beads demonstrated exceptional morphological characteristics. Ionic gelation has proven to be highly effective in the synthesis of biomaterials, yielding a range of spherical hydrogels with improved morphological properties using calcium ions from eggshell-based calcium chloride and sodium alginate from *Sargassum cinctum* (Fig.7 a,b,c). As a baseline formulation that demonstrated the exact control possible in hydrogel matrix synthesis, the experimental series started with a perfect transparent sphere with perfect spherical symmetry and a smooth, glossy surface. Cross-linking sodium alginate and calcium ions through intricate molecular interactions resulted in transparent green hydrogel spheres with a uniform consistency, a sign of a successful ionic gelation process. A cluster of dark olive-green spherical beads, with surface

View Article Online
DOI: 10.1039/D5FB00772K

imperfections that strongly implied the effective encapsulation of *G. sylvestre,* was the final form.

Fig.7 (a) Water sphere (b) *G. sylvestre* sphere (c) *G. sylvestre* beads

3.8 Total Phenol and Flavonoids

The total phenolic content of sphere and bead extracts was 27.77±1.29 and 14.87±0.64 mg GAE/g, respectively, while total flavonoid content was 19.16±0.56 and 6.17±0.17 mg QE/g. These values are substantially lower than those reported for pure *G. sylvestre* aqueous extracts (171.91±1.16 mg GAE/g phenols; 101.07±2.01 mg CE/g flavonoids)[75]. This difference is expected and can be attributed to several factors. The formulations contain sodium alginate (20-30 mg per sphere) and calcium chloride in addition to *G. sylvestre* infusion (2 mL per batch), resulting in a composite matrix where bioactive compounds represent only a fraction of the total dry weight. When expressed per gram of total formulation, the apparent concentration is necessarily lower than pure extract.

3.9 Total Antioxidant Activity

Strong nitric oxide scavenging activity, ranging from 80.12% to 90.79% across dosages of 2–10 mg/mL, demonstrated ascorbic acid's well-known antioxidant potential (Fig.8). Both encapsulated formulations demonstrated notable dose-dependent nitric oxide scavenging properties, with spheres outperforming beads at all tested concentrations. At the maximum concentration of 10 mg/mL, spheres achieved 72.66% scavenging activity, which was 3.02% higher than beads (69.64%), while the pure *G. sylvestre* aqueous extract exhibited comparatively lower activity (52.78%) at the same concentration. Notably, both sphere and bead formulations demonstrated superior antioxidant activity relative to the unencapsulated extract across all tested concentrations, which may be attributed to the combined antioxidant contribution of seaweed-derived sodium alginate. The scavenging percentages for beads increased progressively from 37.91% to 69.64%, while spheres showed a corresponding increase from 43.27% to 72.66%, indicating consistent concentration-dependent antioxidant behaviour in both formulations.

View Article Online
DOI: 10.1039/D5FB00772K

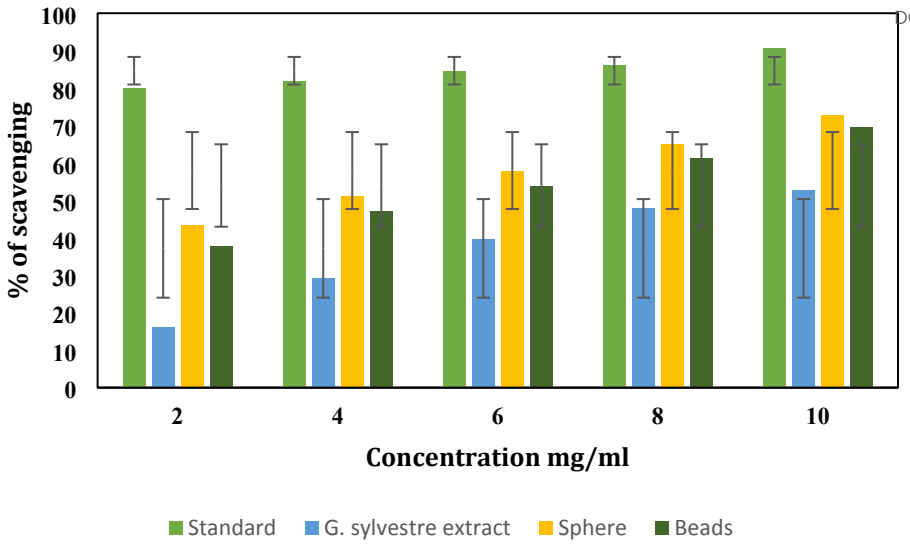

Fig.8 Nitric oxide scavenging activity of spheres and beads

3.10 α-Amylase and α-glucosidase inhibition

Both the sphere and bead formulations demonstrated dose-dependent inhibition of α-amylase and α-glucosidase across the tested concentration range (10–100 µg/mL) (Table-5, Table-6), with statistically significant differences observed between concentration levels ($P < 0.05$). Acarbose, the standard inhibitor, exhibited the highest inhibitory activity against both enzymes, achieving IC_{50} values of 51.58 µg/mL and 47.1 µg/mL for α-amylase and α-glucosidase, respectively. The crude *G. sylvestre* extract demonstrated moderate inhibitory activity, with maximum inhibitions of 83.6 ± 0.36% (α-amylase) and 81.0 ± 0.79% (α-glucosidase) at 100 µg/mL, which were notably lower than those of acarbose but substantially superior to both encapsulated formulations. Among the encapsulated systems, the sphere formulation outperformed the bead formulation marginally, and the bead formulation exhibited the lowest inhibitory activity. A previous study found that a 50% ethanol extract of *G. sylvestre* leaves had inhibitory effects of 18.12 ± 1.05 mg/mL against α-amylase and 20.74 ± 0.74 mg/mL against α-glucosidase[76].

Table -5 α-Amylase inhibition for *G. sylvestre* spheres and beads

Concentration (µg/mL)	α-Amylase Inhibition (%)			
	Acarbose	***G.Sylvestre***	**Sphere**	**Beads**
10	10.2±0.10[a]	7.8±0.10[a]	4.8±0.04[a]	3.4±0.04[a]
25	27.4±0.10[b]	17.7±0.10[b]	9.3±0.51[b]	7.2±0.15[b]
50	42.6±0.15[c]	35.4±0.20[c]	13.6±0.80[c]	11.7±0.15[c]
75	79.3±0.11[d]	62.8±0.76[d]	22.5±0.05[d]	18.4±0.21[d]
100	92.5±0.20[e]	83.6±0.36[e]	30.1±0.45[e]	26.7±0.31[e]
IC_{50} value	**51.58**	**61.86**	**172.09**	**195.02**
F value	**180,750.16**	**19,235.83**	**103,027.98**	**359,479.28**

Results are expressed as mean±S.D. The letters a, b, and c in superscript refer to the significant difference values ($P < 0.05$).

View Article Online
DOI: 10.1039/D5FB00772K

Table -6 α-glucosidase inhibition for *G. sylvestre* spheres and beads

Concentration (µg/mL)	α-glucosidase Inhibition (%)			
	Acarbose	*G.Sylvestre*	Sphere	Beads
10	13.1±0.30[a]	7.06±0.15[a]	4.1±0.03[a]	2.9±0.01[a]
25	34.6±0.36[b]	15.6±0.25[b]	8.9±0.01[b]	6.1±0.03[b]
50	59.3±0.25[c]	27.4±0.36[c]	14.2±0.04[c]	10.2±0.04[c]
75	72.6±0.30[d]	49.3±0.30[d]	24.2±0.03[d]	19.3±0.03[d]
100	91.03±0.49[e]	81.0±0.79[e]	31.1±0.02[e]	28.1±0.01[e]
IC_{50} value	**47.1**	**68.76**	**162.14**	**180.34**
F value	**23,077.41**	**14,080.54**	**332226.52**	**336762.50**

Results are expressed as mean±S.D. The letters a, b, and c in superscript refer to the significant difference values ($P < 0.05$).

3.11 Release Profile Characteristics and pH-Dependent Behaviour

The in vitro release profiles of total phenol and total flavonoid from sphere and bead formulations demonstrated marked pH-dependent behaviour. At pH 1.2, sphere formulations achieved rapid initial release, with 37.34 ± 0.86% phenol released within 30 minutes and 80.53 ± 0.87% by 120 minutes (Table 7). Conversely, bead formulations exhibited longer kinetics, with a total release of 27.80 ± 1.05% at 30 minutes and 58.90 ± 0.30% at 120 minutes, which was 21.6% less than spheres. This formulation-dependent behaviour demonstrates how geometric parameters in matrix-controlled drug delivery systems significantly affect diffusional channel lengths and surface area exposure[54]. At pH 6.8, both formulations exhibited much slower release rates; spheres only released 59.13 ± 0.83% phenol after 180 minutes, while beads released 41.93 ± 0.61% at the same time. When compared to pH 1.2 conditions, this three to four-fold drop in release rate emphasises how crucial environmental pH is in controlling drug-polymer interactions, polymer matrix activity, and compound solubility. Despite being slower, the extended release at pH 6.8 offers substantial physiological advantages by enabling the transport of polyphenols to colonic regions where substantial gut microbiota populations can transform parent compounds into bioactive phenolic acids and metabolites that may have higher bioavailability[77].

Flavonoid release patterns followed similar pH-dependent trends but with notably lower cumulative values across all conditions. At pH 1.2, spheres released 33.47 ± 0.31% flavonoids by 120 minutes, while beads achieved 26.33 ± 0.55% (Table 8). At pH 6.8, release was further attenuated to 42.33 ± 0.57% (spheres) and 36.63 ± 0.45% (beads) by 180 minutes.

Table – 7 Cumulative Release of Phenolic Compounds (µg GAE/100g)

Time (min)	Sphere pH 1.2	Beads pH 1.2	Sphere pH 6.8	Beads pH 6.8
0	0.37±0.15	0.17±0.06	0.6±0.10	0.37±0.06
30	37.34±0.86	27.8±1.05	29.7±0.95	27.67±0.86
60	64.4±0.62	39.5±0.66	37.87±0.81	33.43±0.42
90	75.67±0.71	49.7±0.98	37.67±0.71	32.9±0.44
120	80.53±0.87	58.9±0.30	44.3±0.60	40.53±0.87
150	-	-	47.63±0.74	44.17±0.65
180	-	-	59.13±0.83	41.93±0.61

Results are expressed as mean±S.D.

View Article Online
DOI: 10.1039/D5FB00772K

Table - 8 Cumulative Release of Flavonoid Compounds (µg QE/100g)

Time (min)	Sphere pH 1.2	Beads pH 1.2	Sphere pH 6.8	Beads pH 6.8
0	0.26±0.05	0.20±0.01	0.47±0.04	0.3±0.02
30	3.66±0.06	3.58±0.02	3.90±0.02	3.4±0.03
60	11.37±0.15	6.17±0.11	16.07±0.81	15.7±0.10
90	26.77±0.25	13.53±0.31	23.07±0.35	19.53±0.35
120	33.47±0.31	26.33±0.55	25.8±0.26	23.3±0.46
150	-	-	33.1±0.46	31.23±0.35
180	-	-	42.33±0.57	36.63±0.45

Results are expressed as mean±S.D.

The release profile and antidiabetic activity of the *G. sylvestre* encapsulated formulations were compared with other plant-based encapsulated systems reported in the literature. Ionic gelation-based encapsulation of edible flower extract from *Phlogacanthus thyrsiflorus* using sodium alginate and calcium chloride, optimized via central composite design, achieved an encapsulation efficiency of 72.19 ± 5.19%, with the alginate matrix effectively protecting phenolic compounds from degradation in the acidic gastric phase while facilitating their sustained release under intestinal conditions[78]. This protection pattern is consistent with the release behavior observed in the present study, where both sphere and bead formulations demonstrated progressive phenolic and flavonoid release at pH 6.8 up to 180 minutes. Similarly, *Stevia rebaudiana* aqueous crude extract encapsulated within sodium alginate blends via ionic gelation achieved encapsulation efficiencies ranging from 62.7 to 101.0%, with flavonoids identified as predominant bioactive compounds in the encapsulated fraction and crosslinking conditions significantly influencing phenolic uptake and retention[79]. The considerably higher encapsulation efficiencies reported in both of these studies compared to the present work highlight the importance of systematic bioactive loading optimisation, which is acknowledged as a limitation of this study and proposed for future investigation.

3.12 Mathematical Modelling and Kinetic Analysis

Table - 9 Complete kinetic parameters for spheres and beads

Formulation	Compound	Zero-Order		First-Order		Higuchi		Korsmeyer-Peppas			Best Model
		K_0	R^2	K_1	R^2	KH	R^2	K	n	R^2	Mechanism
Sphere pH 1.2	Phenol	0.6933	0.9651	0.0338	0.9998	7.396	0.9944	0.765	0.9944	0.9998	Anomalous/Higuchi
Beads pH 1.2	Phenol	0.4922	0.9959	0.0171	0.9711	5.223	0.9822	0.621	0.9822	0.9711	Anomalous/Zero-order
Sphere pH 6.8	Phenol	0.1878	0.8598	0.0046	0.7892	3.456	0.9734	0.383	0.9734	0.7892	Fickian/Higuchi

Beads pH 6.8	Phenol	0.1156	0.7234	0.0039	0.6789	2.845	0.8426	0.298	0.8426	0.6789	Fickian/ KP
Sphere pH 1.2	Flavonoid	0.3323	0.9644	0.0256	0.9883	3.126	0.9792	1.635	0.9792	0.9883	Super Case II/Higuchi
Beads pH 1.2	Flavonoid	0.2577	0.9723	0.0189	0.8954	2.876	0.9856	0.894	0.9856	0.8954	Case II/Higuchi
Sphere pH 6.8	Flavonoid	0.2456	0.9623	0.0092	0.9815	3.089	0.9712	1.485	0.9712	0.9815	Super Case II/KP-FI
Beads pH 6.8	Flavonoid	0.2145	0.9456	0.0093	0.8889	3.012	0.9734	0.623	0.9734	0.8889	Anomalous/Higuchi

Units: K_0 (μg/100 g·min^{-1}); K_1 (min^{-1}); KH (μg/100 g·min$^{-1/2}$); K and n (dimensionless)

3.14.1. Zero-Order Kinetics

For phenol release from spheres at pH 1.2, the zero-order rate constant K_0 was 0.6933 μg/100 g·min^{-1} with R^2 = 0.9651, indicating a rather good linear fit(Table 9). Bead formulations displayed K_0 = 0.4922 μg/100 g·min^{-1} (R^2 = 0.9959), a 29% decrease attributed to the reduced surface area and enhanced tortuosity of diffusion channels in the bead morphology[80].

At pH 6.8, zero-order rate constants drastically decreased to 0.1878 μg/100 g·min^{-1} (spheres) and 0.1156 μg/100 g·min^{-1} (beads), suggesting 3.7-fold and 4.3-fold decreases, respectively, demonstrating the substantial influence of pH on release kinetics. Flavonoid release had similar pH sensitivity, but generally lower K_0 values (0.2145–0.3323 μg/100 g·min^{-1}), verifying their more persistent release properties. Even though zero-order kinetics provided appropriate fits in some situations, the different R2 values (0.7234–0.9959) show that concentration-independent release does not fully represent the intricacy of polyphenol transport from these matrix systems. Zero-order kinetics, which preserve pseudo-steady-state conditions throughout release, are frequently observed in matrix systems where drug concentration much surpasses solubility or in reservoir systems with rate-controlling membranes. The deviations of our systems from ideal zero-order behaviour indicate that matrix structural alterations and concentration gradients have an impact on the overall release mechanism[81].

3.14.2. First-Order Kinetics

The first-order model, which explains concentration-dependent release where the rate is proportionate to remaining drug content, showed exceptional applicability, especially at pH 1.2 conditions. At pH 1.2, the first-order rate constant for phenol release from spheres was K_1 = 0.0338 min^{-1} with an excellent R^2 = 0.9998, demonstrating nearly perfect alignment with experimental data (Table 9). Under the rapidly hydrating, highly swollen matrix conditions typical of the gastric environment, this exceptional fit suggests that the release mechanism changes to one where concentration gradients serve as the primary driving force, with the rate of drug release directly proportional to the amount remaining in the matrix at any given time[82].

Bead formulations showed K_1 = 0.0171 min^{-1} (R^2 = 0.9711) for phenol at pH 1.2, which is 49.7% less than spheres. This large difference quantitatively confirms the geometric constraints imposed by bead morphology, which diminish the concentration gradient at the release interface and increase the effective diffusion distance from the matrix core to the

View Article Online
DOI: 10.1039/D5FB00772K

surface. With R2 values between 0.8954 and 0.9883 and first-order constants between 0.0189 and 0.0256 min^{-1} at pH 1.2, flavonoids also demonstrated strong model applicability. The unique exponential approach to complete release observed in various pharmaceutical dose forms is caused by the first-order mechanism, which states that the driving strength for diffusion proportionately decreases as the drug gets farther from the matrix interior. With much lower R2 values (0.6789–0.9815) at pH 6.8, first-order kinetics showed decreased predictive ability, suggesting that variables other than concentration-dependent diffusion affect the release process[83].

3.14.3. Higuchi Model: Universal Descriptor of Diffusion-Controlled Release

At pH 1.2, the Higuchi constant for phenol release from spheres was KH = 7.396 μg/100 $g \cdot min^{-1/2}$ with $R^2 = 0.9944$, whereas beads showed KH = 5.223 μg/100 $g \cdot min^{-1/2}$ ($R^2 = 0.9822$) (Table 9). Because spherical geometry has a bigger surface-to-volume ratio and a shorter radial diffusion channel length than irregular bead forms, spheres have a 41.6% higher Higuchi constant, which quantitatively confirms their superior release efficiency.

Notably, even at pH 6.8, the Higuchi model demonstrated good prediction ability, whereas other models demonstrated less application. At pH 6.8, phenol release from spheres produced KH = 3.456 μg/100 $g \cdot min^{-1/2}$ ($R^2 = 0.9734$), whereas beads displayed KH = 2.845 μg/100 $g \cdot min^{-1/2}$ ($R^2 = 0.8426$). The decreased effective diffusion coefficients resulting from decreased polyphenol solubility, changed matrix characteristics, and possibly stronger drug-polymer interactions at near-neutral pH are quantitatively captured by the pH-dependent decrease in KH values (53% decrease for spheres, 46% decrease for beads). Similar Higuchi kinetics were observed for flavonoid release, with constants ranging from 2.876 to 3.126 μg/100 $g \cdot min^{-1/2}$ at pH 1.2 and 3.012 to 3.089 μg/100 $g \cdot min^{-1/2}$ at pH 6.8, all with $R^2 > 0.97$[84].

3.14.4. Korsmeyer-Peppas Model and Transport Mechanism Classification

According to established criteria for spherical matrices, pure Fickian diffusion is indicated by $n < 0.43$, anomalous (non-Fickian) transport involving coupled diffusion and polymer relaxation is represented by $0.43 < n < 0.85$, Case II transport (relaxation-controlled) is represented by $n = 0.85$, and Super Case II transport, where drug release kinetics exceed polymer relaxation rates, is suggested by $n > 0.85$[85].

Super Case II transport was clearly established by the measurement of phenol release from spheres at pH 1.2, with $n = 0.9944$ ($K = 0.765$, $R^2 = 0.9998$) (Table 8). This extraordinarily high exponent value suggests that matrix degradation and polymer chain relaxation, which happen simultaneously with and may even exceed fundamental diffusional transport, have a major impact on the release process[86]. Bead formulations for phenol at pH 1.2 revealed anomalous transport at the junction of anomalous and Case II processes, with $n = 0.9822$ ($K = 0.621$, $R^2 = 0.9711$). With n values of 0.9734 (spheres) and 0.8426 (beads), phenol release shifted toward more conventional transport methods at pH 6.8. A slightly larger diffusional contribution in relation to polymer relaxation is suggested by the slightly lower exponent when compared to spheres, which may be caused by structural variation in bead matrices that produce areas with varying water penetration and swelling kinetics[87].

Flavonoid release consistently displayed high n values (0.9712–0.9856) under all conditions, indicating Case II or near-Case II transport pathways (Table 9). These higher exponents reflect the complex interplay between the properties of the polymer matrix and the molecular structure of flavonoids. The K values (0.623–1.635) varied considerably between formulations, with higher values at pH 1.2 and for spheres, reflecting both the rate of drug release and the connection between drug transport and polymer structural reorganisation[88].

View Article Online
DOI: 10.1039/D5FB00772K

3.13 Sensory evaluation

In terms of flavour (7.18±0.69) and taste (7.5±0.77), the control formulation, water spheres, fared better than both *G. sylvestre* spheres and beads (Table-10). A novel method for reducing the bitter taste of *G. sylvestre* without compromising its beneficial properties is demonstrated by the sensory examination of spheres and beads infused with the plant. Excellent encapsulation techniques that effectively lessen the herb's characteristic bitterness are demonstrated by the high overall acceptability ratings (8.07–8.5) that counterbalance the relatively lower flavour and taste scores (6.38–7.18). Strong findings for appearance (8.12-8.52), colour (7.95-8.53), and consistency (8.15-8.6) demonstrate that the ionic gelation technique not only decreases sensory problems but also creates spheres that are both visually appealing.

Table -10 Sensory evaluation of Water sphere, *G. sylvestre* sphere, and beads

Parameter	Water Sphere	*G. sylvestre* Spheres	*G. sylvestre* Beads	F value
Colour	7.68 ± 0.40^{a}	8.53 ± 0.63^{b}	7.95 ± 0.59^{a}	18.69
Flavour	7.18 ± 0.69^{b}	6.38 ± 0.74^{a}	6.87 ± 0.52^{b}	11.28
Taste	7.5 ± 0.77^{b}	6.6 ± 0.58^{a}	6.95 ± 0.63^{a}	13.99
Consistency/Texture	8.33 ± 0.62^{a}	8.6 ± 0.61^{b}	8.15 ± 0.62^{a}	4.06
Appearance	8.47 ± 0.82^{a}	8.52 ± 0.69^{a}	8.12 ± 0.55^{a}	2.95
Overall acceptability	8.38 ± 0.74^{b}	6.92 ± 0.66^{a}	7.03 ± 0.76^{a}	38.25

Mean ± S.D (n=3). The letters a, b, and c in superscript refer to the significant difference values ($P < 0.05$). One-way ANOVA confirmed statistically significant differences ($p < 0.05$).

4 Conclusion

This study successfully illustrated an integrated circular bioeconomy framework for converting agricultural and marine biowaste into practical food delivery systems. A multi-stage extraction method produced high-purity calcium chloride (89.14% recovery) from chicken eggshells and sodium alginate (25% efficiency) from *Sargassum cinctum*. Thermogravimetric analysis and FTIR structural characterisation verified their suitability for culinary applications. Ionic gelation facilitated *Gymnema sylvestre*-fortified spheres with pH-responsive release kinetics regulated by Higuchi diffusion mechanisms and Super Case II transport dynamics; phenolic liberation was 80.53% at pH 1.2 and 59.13% at pH 6.8. The formulations exhibited good organoleptic qualities (overall acceptability: 8.07-8.5) and moderate antidiabetic action (30.1% α-amylase, 31.1% α-glucosidase inhibition), despite unresolved bitterness concerns. Optimising bioactive loading through response surface techniques, with food-grade alternatives, carrying out extensive stability and in vivo efficacy studies, and carrying out comprehensive life cycle assessments to assess environmental benefits are priorities for critical advancement. This proof-of-concept not only tackles plastic pollution and produces value cascades from underutilised biomass streams, but it also establishes a promising basis for the creation of sustainable, waste-derived functional food carriers that greatly aid in the circular bioeconomy transitions in food systems.

View Article Online
DOI: 10.1039/D5FB00772K

AUTHOR CONTRIBUTION

- **Uthra B –** Conceptualisation, Methodology, Investigation, Formal analysis, Writing – original draft, Writing – review & editing
- **Dr Paramasivam Raajeswari –** Conceptualisation, Supervision, Project administration, Writing – review & editing

ETHICS DECLARATION

The experimental protocol used was approved by the Human Ethics Committee of the Avinashilingam Institute for Home Science and Higher Education for Women, Coimbatore, Tamil Nadu, India (Approval No. AUW/IHEC/FSN-22-23/XPD-13)

CONSENT FOR PUBLICATION

Informed consent was obtained from all participants.

AVAILABILITY OF DATA AND MATERIALS

The authors confirm that the data supporting the findings of this study are available within the article

FUNDING

This research received no external funding.

CONFLICT OF INTEREST

The authors declare that the research was conducted in the absence of any commercial or financial relationships that could be construed as a potential conflict of interest.

ACKNOWLEDGEMENTS

The author acknowledges the Advanced Research Laboratory and CN. Rao Research Centre, Avinashilingam Institute for Home Science and Higher Education for Women, Coimbatore, for antioxidant assay, FTIR and TGA facility.

Reference

(1) Sharma, S.; Sharma, V.; Chatterjee, S. Contribution of Plastic and Microplastic to Global Climate Change and Their Conjoining Impacts on the Environment - A Review. *Science of The Total Environment* **2023**, *875*, 162627. https://doi.org/10.1016/j.scitotenv.2023.162627.

(2) Cordier, M.; Uehara, T.; Jorgensen, B.; Baztan, J. Reducing Plastic Production: Economic Loss or Environmental Gain? *Camb. prisms Plast.* **2024**, *2*, e2. https://doi.org/10.1017/plc.2024.3.

(3) Walker, T. R.; Fequet, L. Current Trends of Unsustainable Plastic Production and Micro(Nano)Plastic Pollution. *TrAC Trends in Analytical Chemistry* **2023**, *160*, 116984. https://doi.org/10.1016/j.trac.2023.116984.

(4) Patrício Silva, A. L.; Prata, J. C.; Walker, T. R.; Duarte, A. C.; Ouyang, W.; Barcelò, D.; Rocha-Santos, T. Increased Plastic Pollution Due to COVID-19 Pandemic: Challenges and Recommendations. *Chemical Engineering Journal* **2021**, *405*, 126683. https://doi.org/10.1016/j.cej.2020.126683.

(5) Benyathiar, P.; Kumar, P.; Carpenter, G.; Brace, J.; Mishra, D. K. Polyethylene Terephthalate (PET) Bottle-to-Bottle Recycling for the Beverage Industry: A Review. *Polymers* **2022**, *14* (12), 2366. https://doi.org/10.3390/polym14122366.

(6) Pinter, E.; Welle, F.; Mayrhofer, E.; Pechhacker, A.; Motloch, L.; Lahme, V.; Grant, A.; Tacker, M. Circularity Study on PET Bottle-To-Bottle Recycling. *Sustainability* **2021**, *13* (13), 7370. https://doi.org/10.3390/su13137370.

(7) Aslani, H.; Pashmtab, P.; Shaghaghi, A.; Mohammadpoorasl, A.; Taghipour, H.; Zarei, M. Tendencies towards Bottled Drinking Water Consumption: Challenges Ahead of Polyethylene Terephthalate (PET) Waste Management. *Health Promot Perspect* **2021**, *11* (1), 60–68. https://doi.org/10.34172/hpp.2021.09.

(8) Walker, T. R.; Wang, L.; Horton, A.; Xu, E. G. Micro(Nano)Plastic Toxicity and Health Effects: Special Issue Guest Editorial. *Environment International* **2022**, *170*, 107626. https://doi.org/10.1016/j.envint.2022.107626.

(9) Professor and Head of Department of Prosthodontics, Saveetha Dental College and Hospitals, Saveetha Institute of Medical and Technical Sciences, Saveetha University, 162, Poonamallee High Road, Chennai; Ganapathy, D. Awareness Of Hazards Caused By Long-Term Usage Of Polyethylene Terephthalate (PET) Bottles. *IJDOS* **2021**, 2976–2980. https://doi.org/10.19070/2377-8075-21000605.

(10) Da Silva Costa, R.; Sainara Maia Fernandes, T.; De Sousa Almeida, E.; Tomé Oliveira, J.; Carvalho Guedes, J. A.; Julião Zocolo, G.; Wagner De Sousa, F.; Do Nascimento, R. F. Potential Risk of BPA and Phthalates in Commercial Water Bottles: A Minireview. *Journal of Water and Health* **2021**, *19* (3), 411–435. https://doi.org/10.2166/wh.2021.202.

(11) Kibria, Md. G.; Paul, U. K.; Hasan, A.; Mohtasim, Md. S.; Das, B. K.; Mourshed, M. Current Prospects and Challenges for Biomass Energy Conversion in Bangladesh: Attaining Sustainable Development Goals. *Biomass and Bioenergy* **2024**, *183*, 107139. https://doi.org/10.1016/j.biombioe.2024.107139.

(12) Liu, C.; Gao, J.; Jiang, H.; Sun, J.; Gao, X.; Mao, X. Value-added Utilization Technologies for Seaweed Processing Waste in a Circular Economy: Developing a Sustainable Modern Seaweed Industry. *Comp Rev Food Sci Food Safe* **2024**, *23* (6), e70027. https://doi.org/10.1111/1541-4337.70027.

(13) Gandhi, G.; Biswas, K.; Vaghela, P.; Nayak, J.; Nair, A.; Moradiya, K.; Gopalakrishnan, V. A. K.; Veeragurunathan, V.; Ghosh, A. In-Depth Metabolite Characterization of Seaweed-Based Plant Biostimulants: Insights into Bioactive Components. *Algal Research* **2024**, *81*, 103574. https://doi.org/10.1016/j.algal.2024.103574.

(14) Salunke, M.; Mane, P.; Kumbhar, S.; Wakure, B. An Evaluation of Sargassum Cinctum Anticancer Properties Utilizing in Vitro Testing and Molecular Docking, with Assistance from GC-HRMS and FTIR. *J Appl Pharm Sci* **2024**. https://doi.org/10.7324/JAPS.2024.184768.

(15) Frent, O.; Vicas, L.; Duteanu, N.; Morgovan, C.; Jurca, T.; Pallag, A.; Muresan, M.; Filip, S.; Lucaciu, R.-L.; Marian, E. Sodium Alginate—Natural Microencapsulation Material of Polymeric Microparticles. *IJMS* **2022**, *23* (20), 12108. https://doi.org/10.3390/ijms232012108.

(16) Fertah, M.; Belfkira, A.; Dahmane, E. M.; Taourirte, M.; Brouillette, F. Extraction and Characterization of Sodium Alginate from Moroccan Laminaria Digitata Brown Seaweed. *Arabian Journal of Chemistry* **2017**, *10*, S3707–S3714. https://doi.org/10.1016/j.arabjc.2014.05.003.

(17) Jadach, B.; Świetlik, W.; Froelich, A. Sodium Alginate as a Pharmaceutical Excipient: Novel Applications of a Well-Known Polymer. *Journal of Pharmaceutical Sciences* **2022**, *111* (5), 1250–1261. https://doi.org/10.1016/j.xphs.2021.12.024.

(18) Aditya, S.; Stephen, J.; Radhakrishnan, M. Utilization of Eggshell Waste in Calcium-Fortified Foods and Other Industrial Applications: A Review. *Trends in Food Science & Technology* **2021**, *115*, 422–432. https://doi.org/10.1016/j.tifs.2021.06.047.
(19) Ahmed, T. A. E.; Wu, L.; Younes, M.; Hincke, M. Biotechnological Applications of Eggshell: Recent Advances. *Front. Bioeng. Biotechnol.* **2021**, *9*, 675364. https://doi.org/10.3389/fbioe.2021.675364.
(20) Yadav, V. K.; Yadav, K. K.; Cabral-Pinto, M. M. S.; Choudhary, N.; Gnanamoorthy, G.; Tirth, V.; Prasad, S.; Khan, A. H.; Islam, S.; Khan, N. A. The Processing of Calcium Rich Agricultural and Industrial Waste for Recovery of Calcium Carbonate and Calcium Oxide and Their Application for Environmental Cleanup: A Review. *Applied Sciences* **2021**, *11* (9), 4212. https://doi.org/10.3390/app11094212.
(21) Johnson, P.; Aurtherson, P. B.; Suthan, R.; Madhu, S. Experimental Investigation of Pineapple Fiber and Calcinated Poultry Egg Shell Powder Epoxy Composites. *Biomass Conv. Bioref.* **2023**, *13* (5), 4385–4392. https://doi.org/10.1007/s13399-022-03609-4.
(22) Strelec, I.; Peranović, K.; Ostojčić, M.; Aladić, K.; Pavlović, H.; Djerdj, I.; Tatar, D.; Maravić, N.; Skoko, Ž.; Budžaki, S. Eggshell Waste Transformation to Calcium Chloride Anhydride as Food-Grade Additive and Eggshell Membranes as Enzyme Immobilization Carrier. *Green Processing and Synthesis* **2024**, *13* (1), 20230254. https://doi.org/10.1515/gps-2023-0254.
(23) Silva Vanessa; Quintas Celia; Ratao Isabel; Nunes Patricia. Exploring Spherification with Some Foods of the Mediterranean Diet. *Chemical Engineering Transactions* **2023**, *102*, 271–276. https://doi.org/10.3303/CET23102046.
(24) *Handbook of Molecular Gastronomy: Scientific Foundations and Culinary Applications*, First edition.; Burke, R., Ed.; CRC Press: Boca Raton, FL, 2021.
(25) Devangan, S.; Varghese, B.; Johny, E.; Gurram, S.; Adela, R. The Effect of *GYMNEMA SYLVESTRE* Supplementation on Glycemic Control in Type 2 Diabetes Patients: A Systematic Review and Meta-analysis. *Phytotherapy Research* **2021**, *35* (12), 6802–6812. https://doi.org/10.1002/ptr.7265.
(26) Tiwari, P.; Mishra, B. N.; Sangwan, N. S. Phytochemical and Pharmacological Properties of *Gymnema Sylvestre* : An Important Medicinal Plant. *BioMed Research International* **2014**, *2014*, 1–18. https://doi.org/10.1155/2014/830285.
(27) Grgić, J.; Šelo, G.; Planinić, M.; Tišma, M.; Bucić-Kojić, A. Role of the Encapsulation in Bioavailability of Phenolic Compounds. *Antioxidants* **2020**, *9* (10), 923. https://doi.org/10.3390/antiox9100923.
(28) Alallam, B.; Abd Kadir, E.; Dewi, F. R. P.; Yong, Y. K.; Lim, V. Extraction and Characterization of Sodium Alginate from Native Malaysian Brown Seaweed Sargassum Polycystum. *International Journal of Biological Macromolecules* **2025**, *287*, 138552. https://doi.org/10.1016/j.ijbiomac.2024.138552.
(29) Stojanovic, R.; Belscak-Cvitanovic, A.; Manojlovic, V.; Komes, D.; Nedovic, V.; Bugarski, B. Encapsulation of Thyme (*Thymus Serpyllum* L.) Aqueous Extract in Calcium Alginate Beads. *J Sci Food Agric* **2012**, *92* (3), 685–696. https://doi.org/10.1002/jsfa.4632.
(30) Touzout, Z.; Abdellaoui, N.; Hadj-Hamou, A. S. Conception of pH-Sensitive Calcium Alginate/Poly Vinyl Alcohol Hydrogel Beads for Controlled Oral Curcumin Delivery Systems. Antibacterial and Antioxidant Properties. *International Journal of Biological Macromolecules* **2024**, *263*, 130389. https://doi.org/10.1016/j.ijbiomac.2024.130389.
(31) Dobroslavić, E.; Cegledi, E.; Robić, K.; Elez Garofulić, I.; Dragović-Uzelac, V.; Repajić, M. Encapsulation of Fennel Essential Oil in Calcium Alginate Microbeads via Electrostatic Extrusion. *Applied Sciences* **2024**, *14* (8), 3522. https://doi.org/10.3390/app14083522.
(32) Chusak, C.; Balmori, V.; Kamonsuwan, K.; Suklaew, P. O.; Adisakwattana, S. Enhancing Viability of Lactobacillus Rhamnosus GG and Total Polyphenol Content in Fermented Black Goji Berry Beverage Through Calcium–Alginate Encapsulation with Hydrocolloids. *Foods* **2025**, *14* (3), 518. https://doi.org/10.3390/foods14030518.

View Article Online
DOI: 10.1039/D5FB00772K

(33) Zhang, J.; Tang, J.; Shi, S.; He, J.; Liu, W.; Li, Y.; Zeng, X.; Pang, J.; Wu, C. Preparation and Characterization of pH-Sensitive Calcium Alginate Hydrogel Beads as Delivery Carriers for the Controlled Release of Fucoxanthin. *Food Hydrocolloids* **2025**, *163*, 111106. https://doi.org/10.1016/j.foodhyd.2025.111106.

(34) Permatasari, A. A. A. P.; Rosiana, I. W.; Wiradana, P. A.; Lestari, M. D.; Widiastuti, N. K.; Kurniawan, S. B.; Widhiantara, I. G. Extraction and Characterization of Sodium Alginate from Three Brown Algae Collected from Sanur Coastal Waters, Bali as Biopolymer Agent. *Biodiversitas* **2022**, *23* (3). https://doi.org/10.13057/biodiv/d230357.

(35) Supriadi, D.; Milanda, T.; C., A. Y.; Muctaridi; Abdassah, M. CALCIUM CARBONATE ISOLATION FROM EGGSHELL TO MEET PHARMACOPOEIAL STANDARDS AND ITS EFFECTIVENESS AS AN ANTACIDS. *Int J App Pharm* **2023**, 204–209. https://doi.org/10.22159/ijap.2023v15i5.48045.

(36) Thakur, R. J.; Shaikh, H.; Gat, Y.; Waghmare, R. B. Effect of Calcium Chloride Extracted from Eggshell in Maintaining Quality of Selected Fresh-Cut Fruits. *Int J Recycl Org Waste Agricult* **2019**, *8* (S1), 27–36. https://doi.org/10.1007/s40093-019-0260-z.

(37) Aharwar, A.; Parihar, D. K. Talaromyces Verruculosus Tannase Immobilization, Characterization, and Application in Tea Infusion Treatment. *Biomass Conv. Bioref.* **2023**, *13* (1), 261–272. https://doi.org/10.1007/s13399-020-01162-6.

(38) Gautam, N.; Garg, S.; Yadav, S. Underutilized Finger Millet Crop for Starch Extraction, Characterization, and Utilization in the Development of Flexible Thin Film. *J Food Sci Technol* **2021**, *58* (11), 4411–4419. https://doi.org/10.1007/s13197-020-04926-0.

(39) Belattmania, Z.; Kaidi, S.; El Atouani, S.; Katif, C.; Bentiss, F.; Jama, C.; Reani, A.; Sabour, B.; Vasconcelos, V. Isolation and FTIR-ATR and 1H NMR Characterization of Alginates from the Main Alginophyte Species of the Atlantic Coast of Morocco. *Molecules* **2020**, *25* (18), 4335. https://doi.org/10.3390/molecules25184335.

(40) Polat, S.; Sayan, P. Ultrasonic-Assisted Eggshell Extract-Mediated Polymorphic Transformation of Calcium Carbonate. *Ultrasonics Sonochemistry* **2020**, *66*, 105093. https://doi.org/10.1016/j.ultsonch.2020.105093.

(41) *European Directorate for the Quality of Medicines and HealthCare (EDQM). Sodium Alginate. In: European Pharmacopoeia 7.0. Council of Europe; 2010. Monograph No. 0625.*

(42) *United States Pharmacopeia and National Formulary (USP-NF). Sodium Alginate [NF Monograph, CAS 9005-38-3]. United States Pharmacopeial Convention. Https://Store.Usp.Org*.

(43) *United States Pharmacopeia (USP). Calcium Chloride [USP Monograph, CaCl2.2H2O]. United States Pharmacopeial Convention. Https://Store.Usp.Org*.

(44) *United States Pharmacopeia. Food Chemicals Codex, 13th Edition (FCC 13). Sodium Alginate (INS 401); Calcium Chloride. United States Pharmacopeial Convention; 2022. Https://Www.Foodchemicalscodex.Org*.

(45) Sunarharum, W. B.; Kambodji, A. D.; Nur, M. The Physical Properties of Coffee Caviar as Influenced by Sodium Alginate Concentration and Calcium Sources. *IOP Conf. Ser.: Earth Environ. Sci.* **2020**, *475* (1), 012021. https://doi.org/10.1088/1755-1315/475/1/012021.

(46) Bortolini, D. G.; Maciel, G. M.; Haminiuk, C. W. I. Edible Bubbles: A Delivery System for Enhanced Bioaccessibility of Phenolic Compounds in Red Fruits and Edible Flowers. *Innovative Food Science & Emerging Technologies* **2024**, *91*, 103523. https://doi.org/10.1016/j.ifset.2023.103523.

(47) Bontzolis, C. D.; Dimitrellou, D.; Plioni, I.; Kandylis, P.; Soupioni, M.; Koutinas, A. A.; Kanellaki, M. Effect of Solvents on Aniseed Aerial Plant Extraction Using Soxhlet and Ultrasound Methods, Regarding Antimicrobial Activity and Total Phenolic Content. *Food Chemistry Advances* **2024**, *4*, 100609. https://doi.org/10.1016/j.focha.2024.100609.

(48) Ramírez-Brewer, D.; Quintana, S. E.; García-Zapateiro, L. A. Modeling and Optimization of Microwave-Assisted Extraction of Total Phenolics Content from Mango (Mangifera Indica) Peel Using Response Surface Methodology (RSM) and Artificial Neural Networks (ANN). *Food Chemistry: X* **2024**, *22*, 101420. https://doi.org/10.1016/j.fochx.2024.101420.

(49) El Kamari, F.; El Omari, H.; El-Mouhdi, K.; Chlouchi, A.; Harmouzi, A.; Lhilali, I.; El Amrani, J.-E.; Zahouani, C.; Hajji, Z.; Ousaaid, D. Effects of Different Solvents on the Total Phenol Content, Total Flavonoid Content, Antioxidant, and Antifungal Activities of Micromeria Graeca L. from Middle Atlas of Morocco. *Biochemistry Research International* **2024**, *2024*, 1–8. https://doi.org/10.1155/2024/9027997.

(50) Malino, A. P.; Kepel, B. J.; Budiarso, F. D. H.; Fatimawali, F.; Manampiring, A. E.; Bodhi, W. In Vitro Test of Antioxidant Activity of Leilem Leaf Ethanol Extract (Clerodendrum Minahassae) Using DPPH and FRAP Methods. *Heca J. Appl. Sci.* **2024**, *2* (1), 27–34. https://doi.org/10.60084/hjas.v2i1.135.

(51) Xiao, Z.; Yang, R.; Wang, H.; Cui, X.; Zhang, Y.; Yuan, Y.; Yue, T.; Li, P. Inhibitory Properties of Polyphenols in *Malus* "Winter Red" Crabapple Fruit on A-glucosidase and A-amylase Using Improved Methods. *J Food Biochem* **2021**, *45* (10). https://doi.org/10.1111/jfbc.13942.

(52) Xie, F.; De Wever, P.; Fardim, P.; Van Den Mooter, G. TEMPO-Oxidized Cellulose Beads as Potential pH-Responsive Carriers for Site-Specific Drug Delivery in the Gastrointestinal Tract. *Molecules* **2021**, *26* (4), 1030. https://doi.org/10.3390/molecules26041030.

(53) Sawaftah, N. A.; Paul, V.; Awad, N.; Husseini, G. A. Modeling of Anti-Cancer Drug Release Kinetics From Liposomes and Micelles: A Review. *IEEE Trans.on Nanobioscience* **2021**, *20* (4), 565–576. https://doi.org/10.1109/TNB.2021.3097909.

(54) Askarizadeh, M.; Esfandiari, N.; Honarvar, B.; Sajadian, S. A.; Azdarpour, A. Kinetic Modeling to Explain the Release of Medicine from Drug Delivery Systems. *ChemBioEng Reviews* **2023**, *10* (6), 1006–1049. https://doi.org/10.1002/cben.202300027.

(55) Yudiati, E.; Santosa, G. W.; Tontowi, M. R.; Sedjati, S.; Supriyantini, E.; Khakimah, M. Optimization of Alginate Alkaline Extraction Technology from *Sargassum Polycystum* and Its Antioxidant Properties. *IOP Conf. Ser.: Earth Environ. Sci.* **2018**, *139*, 012052. https://doi.org/10.1088/1755-1315/139/1/012052.

(56) Viswanathan, S.; Nallamuthu, T. Extraction of Sodium Alginate from Selected Seaweeds and Their Physiochemical and Biochemical Properties. *International Journal of Innovative Research in Science, Engineering and Technology* **2014**, *3* (4).

(57) Garnjanagoonchorn, W.; Changpuak, A. Preparation and Partial Characterization of Eggshell Calcium Chloride. *International Journal of Food Properties* **2007**, *10* (3), 497–503. https://doi.org/10.1080/10942910600919484.

(58) Domrongpokkaphan, V.; Khemkhao, M. Calcium Chloride Produced from Eggshell for Vegetable Washing. *j.appsci* **2017**, *16* (2), 1–7. https://doi.org/10.14416/j.appsci.2017.09.001.

(59) Irianto, H. E.; Giyatmi, G.; Fransiska, D.; Nuraelah, A. Physical and Chemical Characteristics of Alginate Extracted from Sargassum Sp. *IOP Conf. Ser.: Earth Environ. Sci.* **2023**, *1177* (1), 012029. https://doi.org/10.1088/1755-1315/1177/1/012029.

(60) Rashedy, S. H.; Abd El Hafez, M. S. M.; Dar, M. A.; Cotas, J.; Pereira, L. Evaluation and Characterization of Alginate Extracted from Brown Seaweed Collected in the Red Sea. *Applied Sciences* **2021**, *11* (14), 6290. https://doi.org/10.3390/app11146290.

(61) Latifah, R. N.; Rahmania, S.; Rohmah, B. L. The Effect of Extraction Time on the Quality of Brown Seaweed Na-Alginate Sargassum Polycisteum as the Base Material for SBK Edible Film. *J. Phys.: Conf. Ser.* **2022**, *2190* (1), 012001. https://doi.org/10.1088/1742-6596/2190/1/012001.

(62) Raghul, M. WASTE VALORISATION OF CHICKEN EGG SHELLS AND DEVELOPMENT OF FORMULATED BISCUITS WITH EGG SHELL WASTE AS A SOURCE OF DIETARY CALCIUM. *FENS* **2023**, *22* (1). https://doi.org/10.4316/fens.2023.002.

(63) Wang, W.; Huang, Y.; Pan, Y.; Dabbour, M.; Dai, C.; Zhou, M.; He, R. Sodium Alginate Modifications: A Critical Review of Current Strategies and Emerging Applications. *Foods* **2025**, *14* (22), 3931. https://doi.org/10.3390/foods14223931.

(64) Lai, J.; Azad, A. K.; Sulaiman, W. M. A. W.; Kumarasamy, V.; Subramaniyan, V.; Alshehade, S. A. Alginate-Based Encapsulation Fabrication Technique for Drug Delivery: An Updated Review of

Particle Type, Formulation Technique, Pharmaceutical Ingredient, and Targeted Delivery System. *Pharmaceutics* **2024**, *16* (3), 370. https://doi.org/10.3390/pharmaceutics16030370.

(65) Alallam, B.; Abd Kadir, E.; Dewi, F. R. P.; Yong, Y. K.; Lim, V. Extraction and Characterization of Sodium Alginate from Native Malaysian Brown Seaweed Sargassum Polycystum. *International Journal of Biological Macromolecules* **2025**, *287*, 138552. https://doi.org/10.1016/j.ijbiomac.2024.138552.

(66) Mohammed, A.; Rivers, A.; Stuckey, David. C.; Ward, K. Alginate Extraction from Sargassum Seaweed in the Caribbean Region: Optimization Using Response Surface Methodology. *Carbohydrate Polymers* **2020**, *245*, 116419. https://doi.org/10.1016/j.carbpol.2020.116419.

(67) Aitouguinane, M.; El Alaoui-Talibi, Z.; Rchid, H.; Fendri, I.; Abdelkafi, S.; El-Hadj, M. D. O.; Boual, Z.; Le Cerf, D.; Rihouey, C.; Gardarin, C.; Dubessay, P.; Michaud, P.; Pierre, G.; Delattre, C.; El Modafar, C. Elicitor Activity of Low-Molecular-Weight Alginates Obtained by Oxidative Degradation of Alginates Extracted from Sargassum Muticum and Cystoseira Myriophylloides. *Marine Drugs* **2023**, *21* (5), 301. https://doi.org/10.3390/md21050301.

(68) Martínez-Martínez, E.; Slocum, A. H.; Ceballos, M. L.; Aponte, P.; Bisonó-León, A. G. Beyond the Bloom: Invasive Seaweed Sargassum Spp. as a Catalyst for Sustainable Agriculture and Blue Economy—A Multifaceted Approach to Biodegradable Films, Biostimulants, and Carbon Mitigation. *Sustainability* **2025**, *17* (8), 3498. https://doi.org/10.3390/su17083498.

(69) Helmiyati; Aprilliza, M. Characterization and Properties of Sodium Alginate from Brown Algae Used as an Ecofriendly Superabsorbent. *IOP Conf. Ser.: Mater. Sci. Eng.* **2017**, *188*, 012019. https://doi.org/10.1088/1757-899X/188/1/012019.

(70) Belattmania, Z.; Kaidi, S.; El Atouani, S.; Katif, C.; Bentiss, F.; Jama, C.; Reani, A.; Sabour, B.; Vasconcelos, V. Isolation and FTIR-ATR and 1H NMR Characterization of Alginates from the Main Alginophyte Species of the Atlantic Coast of Morocco. *Molecules* **2020**, *25* (18), 4335. https://doi.org/10.3390/molecules25184335.

(71) Park, Y.; Malgas, S.; Krause, R. W. M.; Pletschke, B. I. Extraction and Characterisation of Sodium Alginate from the Southern African Seaweed *Ecklonia Maxima*. *Botanica Marina* **2024**, *67* (5), 513–523. https://doi.org/10.1515/bot-2024-0011.

(72) Fraissler, G.; Jöller, M.; Brunner, T.; Obernberger, I. Influence of Dry and Humid Gaseous Atmosphere on the Thermal Decomposition of Calcium Chloride and Its Impact on the Remove of Heavy Metals by Chlorination. *Chemical Engineering and Processing: Process Intensification* **2009**, *48* (1), 380–388. https://doi.org/10.1016/j.cep.2008.05.003.

(73) Gaikwad, S. A.; Kulthe, A. A.; Suthar, T. Rc. of flavoured sweet water balls prepared by basic spherification technique. Characterization of Flavoured Sweet Water Balls Prepared by Basic Spherification Technique. *International Journal of chemical studies 7* (1), 1714–1718.

(74) Vipaluk Patomchaiviwat; Pornsak Sriamornsak; Gaysorn Chansiri; Sontaya Limmatvapirat; Anchisa Supawattanakul; Timpika Chonganon; Apinya Keattiteerachai; Suchada Piriyaprasarth. Development of Edible Bubbles of Calcium Alginate for Encapsulating Energy Drinks. *Science* **2022**, *Engineering and Health Studies*, 22050018. https://doi.org/10.14456/SEHS.2022.42.

(75) Kousar, S.; Hussain, A.; Aslam, B.; Faisal, M. N.; Siddique, R.; Sajid, M. R.; Khan, R. U. Synergistic Antioxidant and Antidiabetic Effects of *Caesalpinia Bonduc* (L.) and *Gymnema Sylvestre* (Retz.) in Alloxan-Induced Diabetic Rats. *Chemistry & Biodiversity* **2025**, *22* (9), e202500410. https://doi.org/10.1002/cbdv.202500410.

(76) Katipearachchi, S.; Faizan, M.; Kalansuriya, P.; Attanayake, A. P.; De Silva, N. D. Molecular Docking and In Vitro Assessment of *Gymnema Sylvestre* R. Br. and *Trigonella Foenum-graecum* L. Phytochemicals as Dual α-Amylase and α-Glucosidase Inhibitors. *Chemistry & Biodiversity* **2025**, e01525. https://doi.org/10.1002/cbdv.202501525.

(77) Kardum, N.; Glibetic, M. Polyphenols and Their Interactions With Other Dietary Compounds: Implications for Human Health. In *Advances in Food and Nutrition Research*; Elsevier, 2018; Vol. 84, pp 103–144. https://doi.org/10.1016/bs.afnr.2017.12.001.

(78) Chetia, I.; Tongbram, T.; Ponnam, S. P. G.; Badwaik, L. S. Alginate-Based Encapsulation of Edible Flower Extract: Process Optimization, Characterization and in Vitro Release Kinetics. *International Journal of Biological Macromolecules* **2025**, *333*, 148877. https://doi.org/10.1016/j.ijbiomac.2025.148877.

(79) Arriola, N. D. A.; Chater, P. I.; Wilcox, M.; Lucini, L.; Rocchetti, G.; Dalmina, M.; Pearson, J. P.; De Mello Castanho Amboni, R. D. Encapsulation of Stevia Rebaudiana Bertoni Aqueous Crude Extracts by Ionic Gelation – Effects of Alginate Blends and Gelling Solutions on the Polyphenolic Profile. *Food Chemistry* **2019**, *275*, 123–134. https://doi.org/10.1016/j.foodchem.2018.09.086.

(80) Vanden Braber, N. L.; Paredes, A. J.; Rossi, Y. E.; Porporatto, C.; Allemandi, D. A.; Borsarelli, C. D.; Correa, S. G.; Montenegro, M. A. Controlled Release and Antioxidant Activity of Chitosan or Its Glucosamine Water-Soluble Derivative Microcapsules Loaded with Quercetin. *International Journal of Biological Macromolecules* **2018**, *112*, 399–404. https://doi.org/10.1016/j.ijbiomac.2018.01.085.

(81) Laracuente, M.-L.; Yu, M. H.; McHugh, K. J. Zero-Order Drug Delivery: State of the Art and Future Prospects. *Journal of Controlled Release* **2020**, *327*, 834–856. https://doi.org/10.1016/j.jconrel.2020.09.020.

(82) Lin, Y.-S.; Tsay, R.-Y. Drug Release from a Spherical Matrix: Theoretical Analysis for a Finite Dissolution Rate Affected by Geometric Shape of Dispersed Drugs. *Pharmaceutics* **2020**, *12* (6), 582. https://doi.org/10.3390/pharmaceutics12060582.

(83) Adepu, S.; Ramakrishna, S. Controlled Drug Delivery Systems: Current Status and Future Directions. *Molecules* **2021**, *26* (19), 5905. https://doi.org/10.3390/molecules26195905.

(84) Fitaihi, R. A.; Aleanizy, F. S.; Elsamaligy, S.; Mahmoud, H. A.; Bayomi, M. A. Role of Chitosan on Controlling the Characteristics and Antifungal Activity of Bioadhesive Fluconazole Vaginal Tablets. *Saudi Pharmaceutical Journal* **2018**, *26* (2), 151–161. https://doi.org/10.1016/j.jsps.2017.12.016.

(85) Nissara Ahammed; Sundaramoorthi, R.; Venkatesh Dinnekere Puttegowda; Umashankar Chikkanna. Formulation and Evaluation of Curcumin Coated Central Venous Catheters in the Eradication of Catheter-Related Blood Stream Infections. *J. Appl. Pharm. Res.* **2025**, *13* (3), 233–246. https://doi.org/10.69857/joapr.v13i3.958.

(86) Bulut, E. Chitosan Coated- and Uncoated-Microspheres of Sodium Carboxymethyl Cellulose/Polyvinyl Alcohol Crosslinked with Ferric Ion: Flurbiprofen Loading and in Vitro Drug Release Study. *Journal of Macromolecular Science, Part A* **2020**, *57* (1), 72–82. https://doi.org/10.1080/10601325.2019.1671770.

(87) Archana; Deshmukh, R. Fabrication and Characterization of Andrographolide-Loaded Microsponges to Enhance Oral Bioavailability of Drug against Colon Cancer Using HT29 Cells. *NANOASIA* **2024**, *14* (4), e260724232332. https://doi.org/10.2174/0122106812306507240725114851.

(88) Dardir, F. M.; Ahmed, E. A.; Soliman, M. F.; Othman, S. I.; Allam, A. A.; Alwail, M. A.; Abukhadra, M. R. Synthesis of Chitosan/Al-MCM-41 Nanocomposite from Natural Microcline as a Carrier for Levofloxacin Drug of Controlled Loading and Release Properties; Equilibrium, Release Kinetic, and Cytotoxicity. *Colloids and Surfaces A: Physicochemical and Engineering Aspects* **2021**, *624*, 126805. https://doi.org/10.1016/j.colsurfa.2021.126805.

View Article Online
DOI: 10.1039/D5FB00772K

Data Availability Statement

Gymnema sylvestre-Fortified Spheres and Beads from Waste Biomass: A Circular Bioeconomy Approach for Functional Food Delivery

The authors confirm that the data supporting the findings of this study are available within the article.

Thank you

Sincerely,

Uthra. B

Raajeswari. PA